Recursive formulation and parallel implementation of multiscale mixed methods

E. Abreu[a], P. Ferraz[b,*], A. M. Espírito Santo[c], F. Pereira[d], L. G. C. Santos[b], F. S. Sousa[e]

[a]Instituto de Matemática, Estatística e Computação Científica, Universidade de Campinas, R. Sérgio Buarque de Holanda, 651, 13083-859, Campinas, SP , Brazil
[b]Centro de Estudos do Petróleo, Universidade de Campinas, R. Cora Coralina, 350, 13083-896 Campinas, SP, Brazil
[c]Departamento de MatemÃqtica Pura e Aplicada, Universidade Federal do Rio Grande do Sul, Av. Bento GonÃğalves, 9500, 13083859, Porto Alegre, RS, Brazil
[d]Department of Mathematical Sciences, The University of Texas at Dallas, 800 W. Campbell Road, Richardson, TX 75080-3021, USA
[e]Instituto de Ciências Matemáticas e de Computação, Universidade de São Paulo, Av. Trabalhador São-carlense, 400, 13566-590, São Carlos, SP, Brazil

Abstract

Multiscale methods for second order elliptic equations based on non-overlapping domain decomposition schemes have great potential to take advantage of multi-core, state-of-the-art parallel computers. These methods typically involve solving local boundary value problems followed by the solution of a global interface problem. Known iterative procedures for the solution of the interface problem have typically slow convergence, increasing the overall cost of the multiscale solver. To overcome this problem we develop a scalable recursive solution method for such interface problem that replaces the global problem by a family of small interface systems associated with adjacent subdomains, in a hierarchy of nested subdomains. Then, we propose a novel parallel algorithm to implement our recursive formulation in multi-core devices using the Multiscale Robin Coupled Method by Guiraldello et al. (2018), that can be seen as a generalization of several multiscale mixed methods. Through several numerical studies we show that the new algorithm is very fast and exhibits excellent strong and weak scalability. We consider very large problems, that can have billions of discretization cells, motivated by the numerical simulation of subsurface flows.

Keywords: Recursive Multiscale Robin Coupled Method, Parallelization, Mixed finite elements, Domain decomposition, Fluid Dynamics in Porous Media, Darcy's Law

1. Introduction

Multiscale methods have been developed in the last few decades to approximate efficiently problems involving second order elliptic partial differential equations. These problems are very important in several areas of research, in particular in applications to oil reservoir simulation with high contrast in heterogeneity.

---

*Corresponding author
E-mail Address: paola.ferraz@gmail.com, pferraz@ime.unicamp.br

Despite considerable advances in computational processing capability and storage, traditional methods that have been used in mainstream oil reservoir simulators are not capable of dealing with problems involving billions of elements in the discretization of large computational regions. Very large reservoirs of interest to the industry can be found, for instance, in the Brazilian pre-salt layer and acceptable accuracy in numerical simulations require a considerable number of elements. As more variables and processes are taken into account to accurately resolve fine scale details of real life models, resource efficiency is an important requirement. A number of multiscale methods have been developed to overcome the computational challenges posed by these simulations and ensure acceptable precision of numerical solutions. Domain decomposition techniques divide the global domain into subregions that may be overlapping or non-overlapping, facilitating the use of parallelization techniques. Local solutions, called multiscale basis functions, are constructed through solutions of boundary value problems within each subdomain. These functions retain fine mesh information and are employed as building blocks to construct global approximations for the problem at hand. The key idea is to obtain an approximate solution considering unknowns defined on a coarse scale, and thus reducing drastically the number of unknowns with respect to the fine mesh. The multiscale basis functions are then used to reconstruct the fine scale solution from the coarse problem.

Two major classes of multiscale methods can be identified: methods in the context of finite elements such as the Multiscale Finite Element Methods (MSFE) [1, 2] and the Generalized Multiscale Finite Element Method (GMsFEM) [3], and those that use finite volume such as the Multiscale Finite Volume Methods (MSFV) [4, 5, 6, 7, 8, 9]. On the other hand, extensions of these multiscale methods were formulated to be used as preconditioners in iterative algebraic solvers [10, 11, 12, 13, 14]. The formulation of multiscale methods are frequently naturally parallelizable and some methods were implemented in multi-core CPU/GPU systems (see, [12, 13, 14, 15, 16]). The largest three-dimensional problem considered in these references has 128 million discretization cells, and was run in CPU/GPU clusters. In our work the focus is on the family of multiscale mixed methods composed by the Multiscale Mortar Mixed Finite Element Method (MMMFEM) [17, 18, 19, 20], the Multiscale Hybrid-Mixed Method (MHM) [21, 22, 23], the Multiscale Mixed Method (MuMM) [24, 25] and the Multiscale Robin Coupled Method (MRCM) [26, 27] that has been more recently introduced in the literature. For these methods, the coarse scale is defined by the skeleton of an underlying domain decomposition where the subdomains are coupled using distinct interface conditions. The MMMFEM couples subdomains through a continuous pressure and weak continuity of normal fluxes. Thus, a post-processing step is inevitable to produce velocity fields with continuous normal components on the fine grid. On the other hand the MHM couples subdomains through the imposition of continuous normal flux components, and the pressure is weakly continuous. The MuMM is a multiscale domain decomposition method based on the work of [28] where the Robin boundary conditions are used to obtain local solutions. In the MuMM the continuity of normal component of fluxes as well as the pressure are weakly imposed. Finally, there is the MRCM that also utilizes the Robin coupling conditions between subdomains and generalizes

the above mentioned multiscale mixed approaches. In [26] it is shown that the MMMFEM and MHM can be seen as members of a family of multiscale methods parametrized by the Robin condition coefficient. The MuMM can also be seen as a particular case of the MRCM, when considering piecewise constant spaces set at the skeleton of the decomposition.

Our contribution in this work is twofold. First we introduce a recursive formulation for a family of multiscale mixed methods that is used to construct a new interface solver developed specifically for parallel processing in multi-core systems. The new recursive formulation can be seen as a variational formulation of the procedure recently introduced (and referred to as a multiscale direct solver) in [25]. Then, we propose a novel parallel algorithm based on the recursive formulation. Through a careful analysis for large problems we show that the proposed algorithm is very fast and exhibits excellent scalability, both strong and weak. We consider larger problems as well as larger number of processing cores than in existing parallel results produced by multiscale methods for elliptic equations. For more details of the new recursive approach see [29].

This work is organized as follows. In Section 2 we briefly review the MRCM method. In Section 3 we describe in details the recursive formulation and its parallel implementation. We discuss the connection between the MuMM and the MRCM in Section 4 and in Section 5 we present numerical experiments to show the excellent scalability of our proposed method. In Section 6 we discuss our work with other parallel implementations. Finally, in Section 7 we present our concluding remarks.

2. A review of the Multiscale Robin Coupled Method

The Multiscale Robin Coupled Method (MRCM) introduced in [26] is a multiscale mixed method based on a non-overlapping domain decomposition where subdomains are coupled through weak continuity of pressure and normal across the interfaces between subdomains. The parameter appearing in the Robin condition used in the local boundary value problems associated with the subdomains determines the relative importance of Dirichlet or Neumann boundary condition in the coupling of subdomains. The result is that for small (resp. large) values of this parameter, the solution produced by the MRCM converges to the solution of the MMMFEM (resp. MHM), a property that is well illustrated and explored in [26]. This parameter plays an important role in the approximation of two-phase flows in high-contrast porous media, as can be seen in [30]. Another aspect of this method is that it introduces great flexibility in the choice of interface spaces for normal fluxes and pressures at the skeleton of the decomposition (see [27]). It is also observed in [26] that the variational formulation of the MRCM is an extension of the MuMM, that was originally introduced as an iterative method, and can be recovered by a suitable choice of parameters for the MRCM.

In this section, we recall the key aspects of the MRCM. To briefly introduce the variational formulation,

3

consider a rectangular domain $\Omega \subset \mathbb{R}^d, d \in \{2,3\}$, with a Lipschitz boundary $\partial\Omega$, defined for the following pressure-velocity problem in mixed form,

$$\nabla \cdot \mathbf{u} = f(\mathbf{x}), \qquad \mathbf{u} = -K(\mathbf{x})\nabla p(\mathbf{x}), \qquad \mathbf{x} \in \Omega, \tag{1}$$

$$p = g_D, \qquad \mathbf{x} \in \partial\Omega_D, \tag{2}$$

$$\mathbf{u} \cdot \check{\mathbf{n}} = g_N, \qquad \mathbf{x} \in \partial\Omega_N, \tag{3}$$

where $\mathbf{u} = \mathbf{u}(\mathbf{x})$ is the Darcy's flux and $p(\mathbf{x})$ is the fluid pressure. The absolute permeability is given by $K(\mathbf{x})$, a symmetric positive definite tensor, and $\check{\mathbf{n}}$ is the unit outward normal vector to $\partial\Omega$.

The domain decomposition formulation of the MRCM is performed directly in the discrete form of the system (1)-(3). Thus we start by decomposing the domain Ω into m non-overlapping subdomains Ω^i, $i = 1, \ldots, m$, with reference size H, where

$$\Omega = \bigcup_{i=1}^{m} \Omega^i, \quad \Omega^k \cap \Omega^i = \emptyset, \quad i \neq k, \tag{4}$$

each with a well-defined Lipschitz boundary $\partial\Omega^i$. Let $\Gamma = \cup_i \partial\Omega^i \setminus \partial\Omega$, be the skeleton of the domain decomposition, and

$$\Gamma^i = \Gamma \cap \partial\Omega^i, \quad \Gamma^{ik} = \Gamma^{ki} = \partial\Omega^i \cap \partial\Omega^k. \tag{5}$$

We refer to $\Gamma^{ik} = \Gamma^{ki}$ as the interface between the subdomains Ω^i and Ω^k. Additionally, let us define two types of normal vectors. One denoted by $\check{\mathbf{n}}^i$ is simply the normal vector pointing outward of subdomain Ω^i. The second, denoted as $\check{\mathbf{n}}$ with no superscript, will have a global definition on Γ, that is for every $\Gamma^{ik} \subset \Gamma$, it points towards the subdomain with maximum index value ($\max\{i,k\}$). This will be used as a reference vector in the variational formulation, to uniquely identify the direction of fluxes over each interface of Γ.

Let $\mathcal{T}_h^i$ be a regular mesh discretizing Ω^i, with reference size $h \ll H$ (see Figure 1), where it is possible to define the lowest order Raviart-Thomas spaces for velocity and pressure, say $\mathbf{V}_h^i \subset H(\mathrm{div}, \Omega^i)$ and $Q_h^i \subset L^2(\Omega^i)$, respectively (their definition can be seen in [26]). We will also need the vector space $\mathbf{V}_{h,g_N}^i \subset \mathbf{V}_h^i$ of the functions in $\mathbf{V}_h^i$ satisfying the Neumann boundary conditions in (3).

Finally, the variational formulation of the MRCM introduces unknowns U_H and P_H that are defined only on the skeleton Γ of the domain decomposition. For that purpose, interface spaces are needed, that are defined as subspaces of the set of piecewise constant functions

$$F_h(\mathcal{E}_h) = \{f : \mathcal{E}_h \to \mathbb{R} \mid f|_e \in \mathbb{P}_0, \ \forall e \in \mathcal{E}_h\}, \tag{6}$$

where $\mathcal{E}_h$ is the set of all edges/faces of Γ. Hence, we can take $\mathcal{P}_h = F_h(\mathcal{E}_h)$ as the pressure interface spaces, and $\mathcal{U}_h$ as being the subspace of $F_h(\mathcal{E}_h)$ of the functions that are zero when β^i, the Robin condition parameter defined as a function on $F_h(\mathcal{E}_h)$, vanishes on both sides of the interface. The multiscale formulation of the MRCM is defined over the coarse subspaces $\mathcal{P}_H \subset \mathcal{P}_h$ and $\mathcal{U}_H \subset \mathcal{U}_h$, and formalized below:
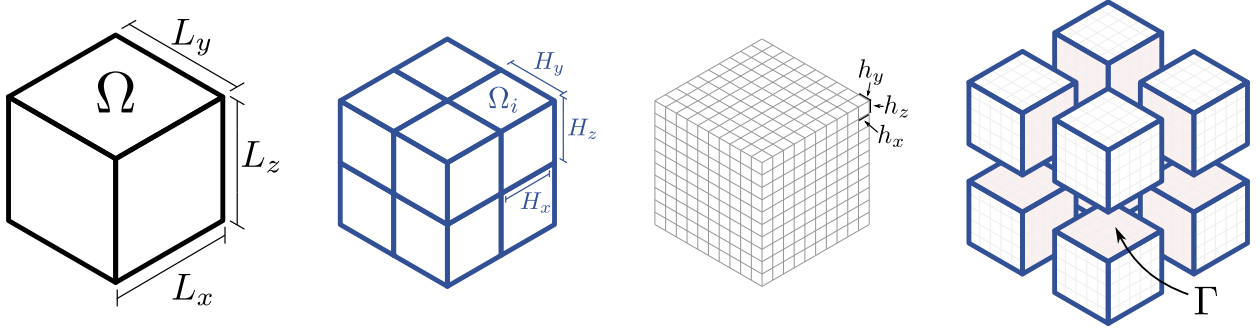
Figure 1: Representations of a three-dimensional domain decomposition of Ω. On the leftmost image, the complete domain is shown with sizes L_x, L_y and L_z. The second and the third pictures show the coarse scale (H) and the fine scale (h), respectively. Rightmost picture depicts Γ, the skeleton of the decomposition and is composed by subdomain interfaces.

Discrete variational formulation of the MRCM. Find the local solution $(\mathbf{u}_h^i, p_h^i) \in \mathbf{V}_{h,g_N}^i \times Q_h^i$, for $i = 1, \ldots, m$, and $(U_H, P_H) \in \mathcal{U}_H \times \mathcal{P}_H$ such that

$$(K^{-1}\mathbf{u}_h^i, \mathbf{v})_{\Omega^i} - (p_h^i, \nabla \cdot \mathbf{v})_{\Omega^i} + (P_H - \beta^i U_H \check{\mathbf{n}}^i \cdot \check{\mathbf{n}} + \beta^i \mathbf{u}_h^i \cdot \check{\mathbf{n}}^i, \mathbf{v} \cdot \check{\mathbf{n}}^i)_{\Gamma^i} = -(g_D, \mathbf{v} \cdot \check{\mathbf{n}}^i)_{\partial\Omega^i \cap \partial\Omega_D} , \qquad (7)$$

$$(q, \nabla \cdot \mathbf{u}_h^i)_{\Omega^i} = (f, q)_{\Omega^i} , \qquad (8)$$

with the following interface conditions

$$\sum_{i=1}^m (\mathbf{u}_h^i \cdot \check{\mathbf{n}}^i, M_H)_{\Gamma^i} = 0 , \qquad (9)$$

$$\sum_{i=1}^m (\beta^i (\mathbf{u}_h^i \cdot \check{\mathbf{n}}^i - U_H \check{\mathbf{n}} \cdot \check{\mathbf{n}}^i), V_H \check{\mathbf{n}}^i \cdot \check{\mathbf{n}})_{\Gamma^i} = 0 , \qquad (10)$$

hold for all $(\mathbf{v}, q) \in \mathbf{V}_{h,0}^i \times Q_h^i$, $\forall i = 1, \ldots, m$, and for all $(V_H, M_H) \in \mathcal{U}_H \times \mathcal{P}_H$.

More details about this variational formulation, as well as the well-posedness of the discrete system, can be seen in [26]. The final global solution $(\mathbf{u}_h, p_h)$ of (1)-(3) is written as a combination of the local solutions $(\mathbf{u}_h^i, p_h^i)$.

2.1. Mixed multiscale basis functions

An efficient implementation of mixed multiscale methods can be achieved by writing the final solution in terms of a set of mixed multiscale basis functions (hereafter referred as MMBF's), a procedure already discussed by other authors, such as Ganis & Yotov [18], Francisco et al. [24] and more recently by Guiraldello et al. [26]. Following the ideas already presented by these authors, especially the later, we recall this procedure to introduce the notation for our recursive formulation of the MRCM.

We start with an additive decomposition of the local solutions $(\mathbf{u}_h^i, p_h^i)$ in Ω^i, as

$$\mathbf{u}_h^i = \widehat{\mathbf{u}}_h^i + \bar{\mathbf{u}}_h^i, \tag{11}$$

$$p_h^i = \widehat{p}_h^i + \bar{p}_h^i, \tag{12}$$

where $(\widehat{\mathbf{u}}_h^i, \widehat{p}_h^i) \in \mathbf{V}_{h,0}^i \times Q_h^i$ represents the homogeneous part, i.e., the solution of the local problem (7)-(8) with given Robin boundary conditions (given U_H and P_H), and vanishing source and external boundary data, while $(\bar{\mathbf{u}}_h^i, \bar{p}_h^i) \in \mathbf{V}_{h,g_N}^i \times Q_h^i$ is the solution of the local problem (7)-(8) with vanishing Robin boundary conditions ($U_H = P_H = 0$), nonzero source, and external boundary data.

The solution of the homogeneous part $(\widehat{\mathbf{u}}_h^i, \widehat{p}_h^i)$ can be obtained as a linear combination of MMBF's, which can be constructed by properly setting U_H and P_H. Consider $\{\phi^j\}_{1 \le j \le n_U}$ and $\{\psi^j\}_{1 \le j \le n_P}$ a finite element basis for the coarse interface spaces $\mathcal{U}_H$ and $\mathcal{P}_H$, respectively, where $n_U = \dim(\mathcal{U}_H)$ and $n_P = \dim(\mathcal{P}_H)$. Then, the interface variables U_H and P_H can be written as

$$U_H = \sum_{j=1}^{n_U} X_j \phi^j, \quad P_H = \sum_{j=1}^{n_P} X_{j+n_U} \psi^j, \tag{13}$$

where the coefficients $X = (X_1, \ldots, X_n)^T$ are to be determined later. Define $\mathcal{J}$ as the set of global indices of the interface degrees of freedom, such that $|\mathcal{J}| = n = n_U + n_P$. Also define $\mathcal{J}^i$ as the set of interface degrees of freedom associated with Ω^i whose support is on the boundary Γ^i, such that $|\mathcal{J}^i| = n^i$. For every $j \in \mathcal{J}^i$, the multiscale basis function in Ω^i, denoted here as $\{\boldsymbol{\Phi}_{k_j}^i, \Psi_{k_j}^i\}_{1 \le k_j \le n^i}$, are given by the following local problems:

- If $1 \le j \le n_U$, solve problem (7)-(8) with boundary data $U_H = \phi^j$, $P_H = 0$:

  Find $(\boldsymbol{\Phi}_{k_j}^i, \Psi_{k_j}^i) \in \mathbf{V}_{h,0}^i \times Q_h^i$, such that

  $$(K^{-1}\boldsymbol{\Phi}_{k_j}^i, \mathbf{v})_{\Omega^i} - (\Psi_{k_j}^i, \nabla \cdot \mathbf{v})_{\Omega^i} + (\beta^i \boldsymbol{\Phi}_{k_j}^i \cdot \check{\mathbf{n}}^i, \mathbf{v} \cdot \check{\mathbf{n}}^i)_{\Gamma^i} = (\beta^i \phi^j \check{\mathbf{n}}^i \cdot \check{\mathbf{n}}, \mathbf{v} \cdot \check{\mathbf{n}}^i)_{\Gamma^i}, \tag{14}$$

  $$(q, \nabla \cdot \boldsymbol{\Phi}_{k_j}^i)_{\Omega^i} = 0, \tag{15}$$

  hold for all $(\mathbf{v}, q) \in \mathbf{V}_{h,0}^i \times Q_h^i$.

- If $n_U < j \le n$, solve problem (7)-(8) with boundary data $U_H = 0$, $P_H = \psi^{j-n_U}$:

  Find $(\boldsymbol{\Phi}_{k_j}^i, \Psi_{k_j}^i) \in \mathbf{V}_{h,0}^i \times Q_h^i$, such that

  $$(K^{-1}\boldsymbol{\Phi}_{k_j}^i, \mathbf{v})_{\Omega^i} - (\Psi_{k_j}^i, \nabla \cdot \mathbf{v})_{\Omega^i} + (\beta^i \boldsymbol{\Phi}_{k_j}^i \cdot \check{\mathbf{n}}^i, \mathbf{v} \cdot \check{\mathbf{n}}^i)_{\Gamma^i} = -(\psi^{j-n_U}, \mathbf{v} \cdot \check{\mathbf{n}}^i)_{\Gamma^i}, \tag{16}$$

  $$(q, \nabla \cdot \boldsymbol{\Phi}_{k_j}^i)_{\Omega^i} = 0, \tag{17}$$

  hold for all $(\mathbf{v}, q) \in \mathbf{V}_{h,0}^i \times Q_h^i$.

In the variational formulations above, the functions ϕ^j and ψ^j depend on the interface space considered. An exploration of several choices for interface spaces, both polynomial and informed spaces, are considered

in [27]. The homogeneous local solutions $(\widehat{\mathbf{u}}_h^i, \widehat{p}_h^i)$ are then written as a linear combination of the multiscale basis functions, $\{\boldsymbol{\Phi}_{k_j}^i, \Psi_{k_j}^i\}_{1 \leq k_j \leq n^i}$, as

$$\widehat{\mathbf{u}}_h^i = \sum_{j \in \mathcal{J}^i} X_j \boldsymbol{\Phi}_{k_j}^i, \qquad \widehat{p}_h^i = \sum_{j \in \mathcal{J}^i} X_j \Psi_{k_j}^i. \tag{18}$$

The local problems (14)-(17) can be solved by any discretization that delivers both pressure and normal fluxes at the skeleton Γ of the decomposition. In [26], the authors perform a conservative finite volume discretization, while in this work, we use the (equivalent) lowest order Raviart-Thomas (RT0) spaces for the interface unknowns, such as in [28, 31, 32, 33, 29]. Although conveniently parallelizable, given the local nature of the problems involved, the computation of a large set of MMBF's can still be very expensive, even in multi-core high-performance computers.

2.2. Interface system

The use of multiscale basis functions allows us to build a linear system for the interface unknowns alone [26, 18, 25]. The procedure consists of substituting the solution (11)-(12) written as a linear combination of the MMBF's (as in (18)) in the coarse scale continuity conditions (9)-(10). The next step is to substitute the interface unknowns by the linear combinations in (13) and test V_H and M_H appearing in (9)-(10) for all basis functions spanning $\mathcal{U}_H$ and $\mathcal{P}_H$. As a result, we end up with a linear system of the form

$$\mathbf{A}\, X = \mathbf{b}, \tag{19}$$

where the unknown vector $X = (X_1, \ldots, X_n)^T$ is formed by the coefficients of the linear combinations in (13). The entries of matrix $\mathbf{A}$ are, for $j = 1, \ldots, n$

$$a_{rj} = \begin{cases} \sum_{i=1}^m \left(\beta^i \left(\boldsymbol{\Phi}_{k_j}^i \cdot \check{\mathbf{n}}^i - \varphi^j \check{\mathbf{n}}^i \cdot \check{\mathbf{n}} \right), \phi^r \check{\mathbf{n}}^i \cdot \check{\mathbf{n}} \right)_{\Gamma^i}, & \text{for } 1 \leq r \leq n_U \\ \sum_{i=1}^m \left(\boldsymbol{\Phi}_{k_j}^i \cdot \check{\mathbf{n}}^i, \psi^r \right)_{\Gamma^i}, & \text{for } n_U < r \leq n \end{cases} \tag{20}$$

where $\varphi^j = \phi^j$ if $1 \leq j \leq n_U$ and zero otherwise. As for the right hand side vector $\mathbf{b}$, computing its entries involves the particular solutions $\bar{\mathbf{u}}_h^i$, yielding

$$\mathbf{b}_r = \begin{cases} -\sum_{i=1}^m (\beta^i \left(\bar{\mathbf{u}}_h^i \cdot \check{\mathbf{n}}^i \right), \phi^r \check{\mathbf{n}}^i \cdot \check{\mathbf{n}})_{\Gamma^i}, & \text{for } 1 \leq r \leq n_U \\ -\sum_{i=1}^m \left(\bar{\mathbf{u}}_h^i \cdot \check{\mathbf{n}}^i, \psi^r \right)_{\Gamma^i}, & \text{for } n_U < r \leq n. \end{cases} \tag{21}$$

Lastly, the local final solution $(\mathbf{u}_h^i, p_h^i)$ in Ω^i, given by (11)-(12), can be written as

$$\mathbf{u}_h^i = \sum_{j \in \mathcal{J}^i} X_j \boldsymbol{\Phi}_{k_j}^i + \bar{\mathbf{u}}_h^i, \qquad p_h^i = \sum_{j \in \mathcal{J}^i} X_j \Psi_{k_j}^i + \bar{p}_h^i. \tag{22}$$

Although quite efficient due to the reduced number of unknowns, this procedure still needs the global assembly and resolution of the non-symmetric linear system (19), that, if not properly done, can hinder the parallel efficiency of the overall method. In the following sections, we will introduce a new naturally parallelizable methodology to localize and decompose the interface problems for maximum efficiency.

7

3. Recursive formulation

We define the recursive formulation for the MRCM in terms of a hierarchy of nested decompositions of the domain Ω where the MRCM is applied recursively. The proposed method approximates the solution of the global problem by the solution of a family of smaller problems that fit well into multi-core parallel machines (see also [29]). The general idea is to start by using the MRCM on a two-subdomain decomposition on Ω, where each subdomain is successively decomposed in two smaller adjacent subdomains until a last stage is reached. The global interface problem is then replaced by a family of small interface systems. For simplicity, in this discussion we assume Ω to be a parallelepiped and all subdomains are cubes.

3.1. A hierarchy of decompositions of the domain Ω

Let us introduce the notation. We define a hierarchy of domain decompositions in level ℓ given by,

$$\Omega = \bigcup_{i=1}^{m^\ell} \Omega^{i,\ell}, \quad m^\ell = 2^\ell, \quad \ell = 0, \ldots, \mathcal{L}. \tag{23}$$

such that in the zero-th level there is no decomposition, i.e., $\Omega^{1,0} = \Omega$. The subdomains of the finest decomposition have sides of size H. To define the hierarchy of decompositions of Ω we define each subdomain of level ℓ as being composed by the union of two subdomains of the decomposition of Ω on level $\ell + 1$,

$$\Omega^{i,\ell} = \Omega^{2i-1,\ell+1} \cup \Omega^{2i,\ell+1}, \quad i = 1, \ldots, m^\ell. \tag{24}$$

For each level ℓ we define $\Gamma^{\cdot,\ell} = \cup_{i=1}^{m^\ell} \partial\Omega^{i,\ell} \setminus \partial\Omega$, as the skeleton of its associated domain decomposition where the "$\cdot$" superscript is to differentiate when the skeleton is defined on levels. We set subdomain interface for each level as $\Gamma^{i,\ell} = \Gamma^{\cdot,\ell} \cap \partial\Omega^{i,\ell}$ (for $\ell = 0$ we have $\Gamma^{\cdot,0} = \emptyset$ by definition) and set $\Gamma^{ik,\ell} = \Gamma^{ki,\ell} = \Omega^{i,\ell} \cap \Omega^{k,\ell}$ as the interface between two subdomains on level ℓ. Also set

$$\gamma^{i,\ell} = \partial\Omega^{2i-i,\ell+1} \cap \partial\Omega^{2i,\ell+1}, \quad i = 1, \ldots, m^\ell, \tag{25}$$

as the interface between two subdomains on level $\ell + 1$ that compose $\Omega^{i,\ell}$ on level ℓ, such that we are able to write the skeleton of the decomposition on each level as

$$\Gamma^{\cdot,\ell+1} = \Gamma^{\cdot,\ell} \cup \left(\bigcup_{i=1}^{m^\ell} \gamma^{i,\ell} \right), \quad \ell = 0, \ldots, \mathcal{L}. \tag{26}$$

For the interface spaces $\mathcal{U}_H$ and $\mathcal{P}_H$, we consider a finite element basis functions $\{\phi^j\}_{1 \leq j \leq n_U}$ and $\{\psi^j\}_{1 \leq j \leq n_P}$ on the skeleton of the *finest* decomposition $\Gamma^{\cdot,\mathcal{L}}$ such that they have support on faces with size $H \times H$. In the recursive formulation, we define $\mathcal{J}^{\cdot,\ell}$ as the total set of indices of interface degrees of freedom on level ℓ, such that

$$\mathcal{J}^{\cdot,0} \subset \ldots \subset \mathcal{J}^{\cdot,\ell} \subset \ldots \subset \mathcal{J}^{\cdot,\mathcal{L}}. \tag{27}$$

We also define $\mathcal{J}^{i,\ell}$ as the set of interface degrees of freedom associated with $\Omega^{i,\ell}$ whose support is on the boundary $\Gamma^{i,\ell}$, such that $|\mathcal{J}^{i,\ell}| = n^{i,\ell}$. Lastly, define $\xi^{i,\ell}$ as the interface degrees of freedom whose support is on $\gamma^{i,\ell}$. Figure 2 shows a two-level domain decomposition sequence and its interfaces. Now we are ready to define the recursive formulation of (7)-(10) to find the approximate solution $(\mathbf{u}_h, p_h)$ of (1)-(3).
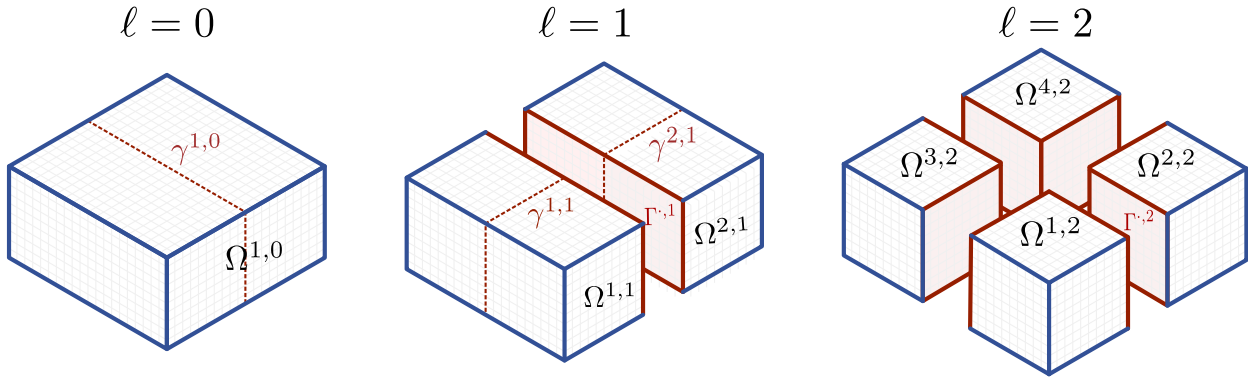

Figure 2: Representation of a sequence of domain decompositions form left to right. We begin at level 0 with the whole domain, where we will perform a Recursive MRCM step over $\gamma^{1,0}$, decomposing the domain into two subdomains. At level 1, we have the subdomains $\Omega^{1,1}$ and $\Omega^{2,1}$, with skeleton $\Gamma^{\cdot,1}$. At this level, we perform two steps of the Recursive MRCM on each subdomain over $\gamma^{1,1}$ and $\gamma^{2,1}$ with each subdomain decomposed into two new subdomains. We reach the finest level 2, where we have the *finest* subdomain mesh with four subdomains and skeleton of the decomposition $\Gamma^{\cdot,2}$.

3.2. Recursive formulation

The recursive formulation consists of the following steps. Approximate (1)-(3) by the MRCM where the domain Ω is decomposed in two subdomains. Within this decomposition, a family of MMBFs has to be computed for each subdomain $\Omega^{i,1}, i = 1, 2$. For each subdomain of level ℓ, $\ell \geq 2$, we follow the same procedure within $\Omega^{i,\ell}$, $i = 1, \ldots, m^\ell$ subdomains. Then, the MMBFs are computed by the use of the MRCM restricted to each $\Omega^{i,\ell}$, $i = 1, \ldots, m^\ell$. This is achieved by decomposing $\Omega^{i,\ell}$ into two smaller subdomains and following the usual steps of the MRCM for a two-subdomain decomposition. We proceed from coarser ($\ell = 0$) to finer decompositions ($\ell = \mathcal{L}$) by approximating the local problems by the MRCM, until the *finest* decomposition is reached. At this point in the formulation we approximate the solution of the MMBFs using a mixed finite element method (MFEM) or equivalently, a finite volume method (FVM). We define the recursive formulation of the MRCM in terms of a hierarchy of nested decompositions of Ω where the MRCM is applied recursively. We refer to this formulation as the Recursive MRCM, and it is introduced in Algorithm 1. Next we discuss Algorithm 1 in detail.

Algorithm 1: Recursive formulation for the MRCM

---

1 **Function** RecMRCM($\Omega^{i,\ell}$)

2   **if** $\ell = \mathcal{L}$ **then**

3   Compute $\{\boldsymbol{\Phi}_s^{i,\mathcal{L}}, \Psi_s^{i,\mathcal{L}}\}_{1 \le s \le n^{i,\mathcal{L}}}$ and $(\bar{\mathbf{u}}^{i,\mathcal{L}}, \bar{p}^{i,\mathcal{L}})$ on $\Omega^{i,\ell}$ via MFEM

4   **return** $(\{\boldsymbol{\Phi}_s^{i,\mathcal{L}}, \Psi_s^{i,\mathcal{L}}\}, \bar{\mathbf{u}}^{i,\mathcal{L}}, \bar{p}^{i,\mathcal{L}})$

5   **else**

6   Define $i_1 = 2i - 1$ and $i_2 = 2i$

7   Decompose $\Omega^{i,\ell} = \Omega^{i_1,\ell+1} \cup \Omega^{i_2,\ell+1}$

8 $\{\boldsymbol{\Phi}_k^{i_1,\ell+1}, \Psi_k^{i_1,\ell+1}\}_{1 \le k \le n^{i_1,\ell+1}}$ and $(\bar{\mathbf{u}}^{i_1,\ell+1}, \bar{p}^{i_1,\ell+1}) \leftarrow$ RecMRCM($\Omega^{i_1,\ell+1}$)

9 $\{\boldsymbol{\Phi}_k^{i_2,\ell+1}, \Psi_k^{i_2,\ell+1}\}_{1 \le k \le n^{i_2,\ell+1}}$ and $(\bar{\mathbf{u}}^{i_2,\ell+1}, \bar{p}^{i_2,\ell+1}) \leftarrow$ RecMRCM($\Omega^{i_2,\ell+1}$)

10   Compute the coefficients $X_s^{i,\ell}$ and $\bar{X}^{i,\ell}$ by solving (19) on $\gamma^{i,\ell}$.

11   **if** $\ell \neq 0$ **then**

12   Compute $\{\boldsymbol{\Phi}_s^{i,\ell}, \Psi_s^{i,\ell}\}_{1 \le s \le n^{i,\ell}}$ and $(\bar{\mathbf{u}}^{i,\ell}, \bar{p}^{i,\ell})$ on $\Omega^{i,\ell}$ with (31)-(32)

13   **return** $(\{\boldsymbol{\Phi}_s^{i,\ell}, \Psi_s^{i,\ell}\}, \bar{\mathbf{u}}^{i,\ell}, \bar{p}^{i,\ell})$

14   **else**

15   Compute $(\mathbf{u}_h, p_h)$ on Ω with (31)-(32)

16   **return** $(\mathbf{u}_h, p_h)$

We begin by defining $(\mathbf{u}^{i,\ell}, p^{i,\ell})$ as the solution of the local problems (7)-(10) restricted to $\Omega^{i,\ell}$. The solution is obtained by following the additive decomposition of the MRCM, only now it is defined for each level: $\mathbf{u}^{i,\ell} = \widehat{\mathbf{u}}^{i,\ell} + \bar{\mathbf{u}}^{i,\ell}$ and $p^{i,\ell} = \widehat{p}^{i,\ell} + \bar{p}^{i,\ell}$. In each $\Omega^{i,\ell}$ we need to compute a set of associated MMBFs. First, let us denote the set of MMBFs in $\Omega^{i,\ell}$ by

$$(\boldsymbol{\Phi}_s^{i,\ell}, \Psi_s^{i,\ell}), \quad s = 1, \dots, n^{i,\ell}, \quad i = 1, \dots, m^{\ell}. \tag{28}$$

At each level, the MMBFs are obtained by the solution of the local problems (14)-(17) on $\Omega^{i,\ell}$. Remember that a particular local solution, $(\bar{\mathbf{u}}^{i,\ell}, \bar{p}^{i,\ell})$, is also needed in order to complete the additive decomposition. The recursive MRCM algorithm can be described as follows: Consider $\Omega^{i,\ell}$, a generic subdomain of level ℓ. We want to compute the MMBFs and the particular solution, $\{(\boldsymbol{\Phi}_s^{i,\ell}, \Psi_s^{i,\ell}), (\bar{\mathbf{u}}^{i,\ell}, \bar{p}^{i,\ell})\}$, $s = 1, \dots, n^{i,\ell}$, associated with this subdomain. If $\ell \neq \mathcal{L}$, then we decompose $\Omega^{i,\ell}$ into $\Omega^{2i-i,\ell+1}$ and $\Omega^{2i,\ell+1}$, as shown in

Figure 3, and compute their associated MMBFs,

$$\{(\boldsymbol{\Phi}_k^{2i-i,\ell+1}, \Psi_k^{2i-i,\ell+1}), \bar{\mathbf{u}}^{2i-i,\ell+1}, \bar{p}^{2i-i,\ell+1}\}, \qquad k = 1, \ldots, n^{2i-i,\ell+1} \tag{29}$$

$$\{(\boldsymbol{\Phi}_k^{2i,\ell+1}, \Psi_k^{2i,\ell+1}), \bar{\mathbf{u}}^{2i,\ell+1}, \bar{p}^{2i,\ell+1}\}, \qquad k = 1, \ldots, n^{2i,\ell+1}, \tag{30}$$

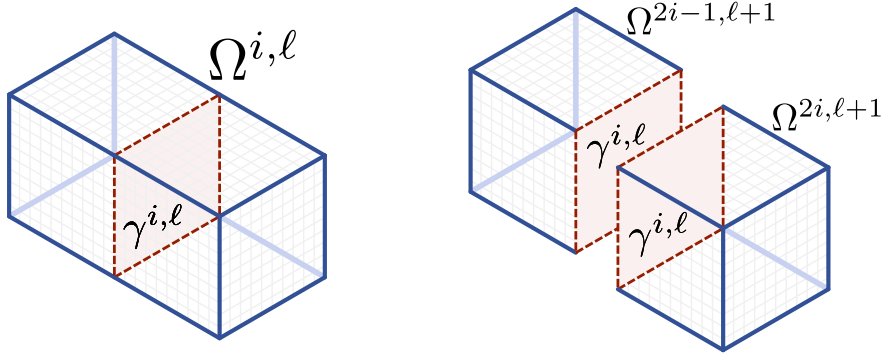in $\Omega^{2i-i,\ell+1}$ and $\Omega^{2i,\ell+1}$, respectively.

Figure 3: The representation of a subdomain $\Omega^{i,\ell}$ in level ℓ, in which a step of the Recursive MRCM will be performed over $\gamma^{i,\ell}$. Local problems are defined in the new subdomains $\Omega^{2i-i,\ell+1}$ and $\Omega^{2i,\ell+1}$.

To compute (29) and (30) we apply the MRCM again, decomposing each subdomain in level $\ell+1$ into two smaller subdomains and computing its MMBFs and particular solution as above. This continues until $\ell = \mathcal{L}$, where (29) and (30) are computed by MFEM. It is important to notice that for $\ell = 0$ we do not compute MMBFs, but the actual approximate solution $(\mathbf{u}_h, p_h)$. To complete the algorithm we need to compute, for each MMBF (and a particular solution) on $\Omega^{i,\ell}$ a set of coefficients $X^{i,\ell}$ (resp. $\bar{X}^{i,\ell}$, for the particular local solution) in $\gamma^{i,\ell}$ by solving an interface linear system given by (19) in the case of two subdomains. Then $(\boldsymbol{\Phi}_s^{i,\ell}, \Psi_s^{i,\ell}, \bar{\mathbf{u}}^{i,\ell}, \bar{p}^{i,\ell})$, $s = 1, \ldots, n^{i,\ell}$, are computed by a linear combination of (29)-(30) with its respective coefficients given by $X_s^{i,\ell}$ and $\bar{X}^{i,\ell}$.

Let us now explain how to compute the MMBFs from the linear combination of MMBFs of subsequent levels. Suppose we already computed the MMBFs of $\Omega^{2i-i,\ell+1}$ and $\Omega^{2i,\ell+1}$ and its associated coefficients $X^{i,\ell}, \bar{X}^{i,\ell}$ on level $\ell+1$. Then, each MMBFs on $\Omega^{i,\ell}$ is computed by

$$\boldsymbol{\Phi}_s^{i,\ell} = \sum_k X_{k,s}^{i,\ell} \boldsymbol{\Phi}_k^{2i-1,\ell+1} + \bar{\mathbf{u}}^{2i-1,\ell+1} + \sum_k X_{k,s}^{i,\ell} \boldsymbol{\Phi}_k^{2i,\ell+1} + \bar{\mathbf{u}}^{\ell+1,2i} + \phi^r \boldsymbol{\Phi}_r^{2i,\ell+1}, \tag{31}$$

$$\Psi_s^{i,\ell} = \sum_k X_{k,s}^{i,\ell} \Psi_k^{2i-1,\ell+1} + \bar{p}^{2i-1,\ell+1} + \sum_k X_{k,s}^{i,\ell} \Psi_k^{2i,\ell+1} + \bar{p}^{2i,\ell+1} + \phi^r \Psi_r^{2i,\ell+1}, \tag{32}$$

where $s \in \{1, \ldots, n^{i,\ell}\}$ and $k \in \{1, \ldots, \xi^{i,\ell}\}$; $\xi^{i,\ell}$ is the number of interface degrees of freedom on $\gamma^{i,\ell}$. The last terms in (31) and (32) are related to the MMBF $(\boldsymbol{\Phi}_r^{2i,\ell+1}, \Psi_r^{2i,\ell+1})$ on $\Omega^{2i,\ell+1}$ that accounts for the

contribution of the boundary value ϕ^r in $\Gamma^{i,\ell}$, as illustrated in the right figure in Figure 4. The particular solution can also be written as a linear combination similar to (31)-(32),

$$\bar{\mathbf{u}}^{i,\ell} = \sum_k \bar{X}_k^{i,\ell} \mathbf{\Phi}_k^{2i-1,\ell+1} + \bar{\mathbf{u}}^{2i-1,\ell+1} + \sum_k \bar{X}_k^{i,\ell} \mathbf{\Phi}_k^{2i,\ell+1} + \bar{\mathbf{u}}^{2i,\ell+1}, \tag{33}$$

$$\bar{p}^{i,\ell} = \sum_k \bar{X}_k^{i,\ell} \Psi_k^{2i-1,\ell+1} + \bar{p}^{2i-1,\ell+1} + \sum_k \bar{X}_k^{i,\ell} \Psi_k^{2i,\ell+1} + \bar{p}^{2i,\ell+1}, \tag{34}$$
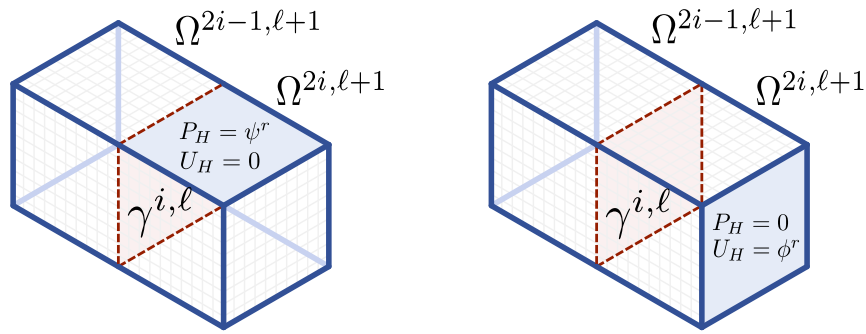
where $k \in \{1, \ldots, \xi^{i,\ell}\}$.

Figure 4: Representation of two boundary conditions of two different MMBFs in $\Omega^{i,\ell}$. This subdomain is composed of $\Omega^{2i-i,\ell+1}$ and $\Omega^{2i,\ell+1}$. The MMBFs of $\Omega^{i,\ell}$ are obtained by alternating the values of U_H and P_H on the external interfaces boundaries $\Gamma^{i,\ell}$, for their finite element basis ϕ^j and ψ^j, as in (14)-(17). On the left figure, the value of $P_H = \psi^r$ is the contribution of that particular coarse interface. On the right figure, the value of $U_H = \phi^r$ is the contribution of that particular coarse interface. The MMBFs in $\Omega^{i,\ell}$ are obtained by the linear combinations (31)-(32).

Remark: This recursive construction of the approximate solution of (1)-(3) by the MRCM allows us to decompose the global interface linear system (19) into a set of small and localized interface linear systems on $\gamma^{i,\ell}$ for all subdomains i and all levels ℓ. Each set of local linear systems on $\gamma^{i,\ell}$ has size $\xi^{i,\ell} \times \xi^{i,\ell}$. The linear systems are independent of each other and can be solved simultaneously. The matrix and right hand side of the local interface systems are constructed using (19) restricted to $\gamma^{i,\ell}$. One important aspect of the algorithm described here is that it can keep track of the coefficients of the linear combinations that are used to express each MMBF of each level as a linear combination of the MMBfs of the previous levels, in a way that we do not need to store all the values of the MMBFs in *coarser* levels. As we proceed to *coarser* levels, those MMBFs can be expressed as linear combinations of the MMBFs associated with the *finest* decomposition ($\ell = \mathcal{L}$). This way, for any given level, we are able to express each multiscale basis function as a linear combination of the *finest* level MMBFs.

4. Parallel Implementation and connection to the Multiscale Mixed Method

The flexibility in the choice of interface spaces for pressure and normal fluxes provided by the MRCM framework comes with a cost. Even if piecewise constant spaces are selected for both variables in a three-dimensional (resp. two-dimensional) subdomain the minimum number of MMBFs that need to be computed in each subdomain is 12 (resp. 8). The problems we intend to solve using the recursive framework will involve up to billions of cells. Thus, we wish to perform simulations with methods that are as inexpensive as possible from the computational point of view. In this context we will implement the recursive procedure in a particular case of MRCM: the Multiscale Mixed Method (MuMM). In implementing the MuMM one need only a set of six (resp. four) MMBFs, in three (resp. two) dimensions, thus reducing the computational cost of the implementation. An important feature of the MuMM is the introduction of an intermediate coarse scale of size $\bar{H}$, such that $h \leq \bar{H} \leq H$, where we define the interface space $F_{\bar{H}} \subset F_h(\mathcal{E}_h)$. This space is taken to be piecewise constant in the $\bar{H}$ scale, see Figure 5.
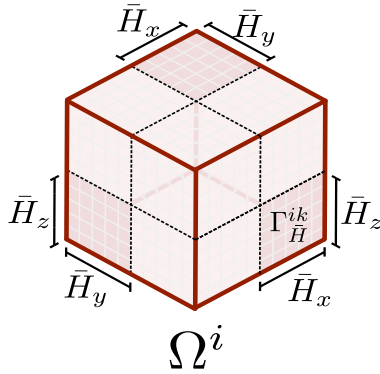
Figure 5: Representation of $\bar{H}$ scale.

Let us define $\Gamma_{\bar{H}}^{ik}$ as one element of the partition of Γ, with size $\bar{H}$, adjacent to subdomains Ω^i and Ω^k, such that $H/\bar{H}$ and $\bar{H}/h$ are both integer numbers. This partition can also be performed independently for each direction, with minor modifications. The introduction of an intermediate scale does not changes the recursive formulation construction, it only adds a flexibility in the number of MMBFs and in the size of the interface linear system to be computed. Since the continuity equations in Γ are defined in the coarse scale, flux conservation is only satisfied in this scale. Downscaling (or smoothing) techniques should be used to recover flux conservation on fine scale [24, 25, 26, 34].

The recursive formulation was implemented in C, C++ and openMPI. To compute the MMBFs and particular for each subdomain of level $\ell = \mathcal{L}$, we use a Mixed Finite Element discretization with lowest index Raviart-Thomas spaces [33] to construct a linear system for the pressure variable. The solution was obtained by means of a conjugate gradient with an algebraic multigrid preconditioner C++ solver, with a tolerance of 10^{-8} [35]. The interface linear systems were solved by a simple, in-house implemented LU solver

since its matrix can be quite small (depending on the choice of the size of the $\bar{H}$ scale) and are efficiently computed by such solver. The recursive formulation is implemented considering a decomposition of the domain such that each direction is decomposed in a power of two. This simplifies the implementation of the message passing between subdomains.

The exchange of information between subdomains is done by keeping the same number of message passing steps constant at each level. This is achieved by a one-to-one message passing between the processing cores that compose a subdomain at a given level. This is illustrated in Figure 6. All our experiments were done on the Santos Dumont cluster located at the National Laboratory for Scientific Computing (LNCC) in Petrópolis, RJ, Brazil, from several million to 2 billion cells on a dual-socket Intel Xeon E5-2695-v2, 2,4GHZ, 64GB DDR3 RAM.
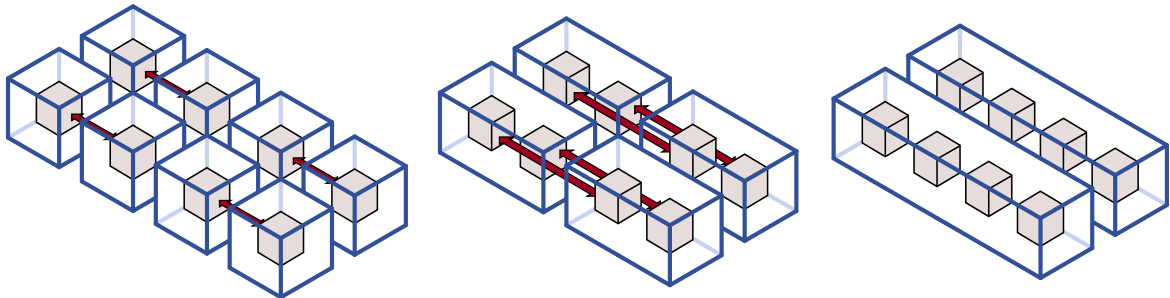
Figure 6: Representation of the message passing pattern between cores (red arrows) in the union operations, as seen in Section 3. In the first level the cores (represented by the grey cubes) and subdomain (represented by shallow blue cubes) meshes are the same. The communication is done with their direct adjacent subdomain. However, in the coarse levels the cores that compose a new subdomain communicate with the cores that are in the same "position" inside the new adjacent subdomain.

5. Numerical Experiments: Setup, Results and Discussions

5.1. Setup for the numerical experiments

In this section, we present numerical experiments to evaluate the computational efficiency and the accuracy of solution of our three-dimensional parallel implementation of the recursive formulation for very large problems, up to 2 billion cells.

We consider the pressure-velocity problem (1)-(3), for a physical domain $[0, L_x] \times [0, L_y] \times [0, L_z]$ and isotropic absolute permeability tensors. Our implementation is based on the MuMM [24], where the interface spaces are piecewise constant functions, as explained in Section 4. For every $\Gamma_{\bar{H}}^{ik}$, the Robin parameter β^i and β^k are chosen to be constant both defines as

$$\beta^i = \beta^k = \frac{\alpha \bar{H}}{\bar{K}_{eff}},$$

(35)

14

where α is a dimensionless parameter [26, 24, 27] and $\bar{K}_{eff}$ is the average of all harmonic means of the adjacent permeabilities in the cells that compose the $\bar{H}$ scale, i.e.,

$$\bar{K}_{eff} = \frac{1}{N} \sum_{e \in \Gamma_{\bar{H}}^{ik}} \frac{2K_e^i K_e^k}{K_e^i + K_e^k}, \tag{36}$$

the sum is on all e cells that compose the $\Gamma_{\bar{H}}^{ik}$.

As discussed before, the magnitude of α controls the coupling between the subdomains, as explained in [26]. The choice of large α values gives higher priority to flux continuity over pressure continuity of the final solution. For the scalability studies we choose a constant value $\alpha = 10^3$ and for the accuracy results we choose $\alpha = 10^6$. The number of operations of the recursive algorithm remains the same and therefore we do not expect its scalability to be affected by the α value (for more details on how the magnitude of α affects the solution, see [27]).

The computational efficiency is evaluated in two cases, namely: i) homogeneous permeability field and ii) high contrast heterogeneous permeability field. For both cases we perform scalability studies where we assess the behavior of the numerical method relative to its computational time against an increasing number of cores. The first scalability test is the strong scaling, where the total number of discretization elements and problem size is fixed while increasing the total number of processing cores. The second scalability test is the weak scaling, where the total size of the problem is increased, while increasing the number of processing cores. We keep the size of the local linear systems in each subdomain constant, while increasing the overall problem size and processing cores, therefore the expected simulation time should remain constant throughout the weak scaling tests. The boundary conditions are given by $p(0, y, z) = 1$ and $p(L_x, y, z) = 0$, combined with no-flow conditions on the other boundaries. For the weak scaling case, boundary conditions are updated in each case, in order to keep the same overall flux, making sure the Darcy problem stays the same, at least for the homogeneous permeabilities.

In the recursive algorithm we need to establish the mesh for the finest domain decomposition, so that we associate each subdomain in level $\ell = \mathcal{L}$ with a unique core. In all our experiments, we define the finest decomposition with no divisions on the z-direction. The implementation considers domain decompositions where each direction is decomposed in a power of two. Tables 1 and 2 organizes the scaling experiments, showing the subdomain divisions and number of cells for the strong and weak scaling studies.

Next, we need to define the size of the coarse $\bar{H}$ partition. For the experiments we use two sets of coarse scale in each $\Omega^{i,\mathcal{L}}$: $\bar{H}_x = H_x$, $\bar{H}_y = H_y$, and $\bar{H}_x = H_x/4$, $\bar{H}_y = H_y/4$; for the coarse scale in the z-direction, we fixed $\bar{H}_z = H_z$. The number of $\bar{H}$ partitions on $\Gamma^{i,\mathcal{L}}$ is the number of MMBFs to be directly computed on the finest decomposition by HMFEM, and it defines the number of MMBFs on all levels through (31)-(32). Table 3 shows, for each coarse scale partition chosen, the total number of MMBFs and particular solution to be computed with HMFEM for all subdomains in the last level. The direct computation of local problems

Table 1: Setup for the scaling experiments with up to 134 million cells (strong scaling) and 268 million cells (weak scaling).

	Strong Scaling			Weak Scaling	
	~ 134 million in Ω			~ 262 thousand in each Ω^i	
Cores (subdomains)		Total cells in Ω^i	Cores (subdomains)		Total cells in Ω
32	$(4 \times 8 \times 1)$	$128 \times 64 \times 512$	32	$(4 \times 8 \times 1)$	8.39×10^6
64	$(8 \times 8 \times 1)$	$64 \times 64 \times 512$	64	$(8 \times 8 \times 1)$	1.68×10^7
128	$(8 \times 16 \times 1)$	$64 \times 32 \times 512$	128	$(8 \times 16 \times 1)$	3.36×10^7
256	$(16 \times 16 \times 1)$	$32 \times 32 \times 512$	256	$(16 \times 16 \times 1)$	6.71×10^7
512	$(16 \times 32 \times 1)$	$32 \times 16 \times 512$	512	$(16 \times 32 \times 1)$	1.34×10^8
1024	$(32 \times 32 \times 1)$	$16 \times 16 \times 512$	1024	$(32 \times 32 \times 1)$	2.68×10^8

Table 2: Setup for the scaling experiments with up to 1 billion cells (strong scaling) and 2 billion cells (weak scaling).

	~ 1 billion in Ω			~ 2 million in each Ω^i	
Cores (subdomains)		Total cells in Ω^i	Cores (subdomains)		Total cells in Ω
			32	$(4 \times 8 \times 1)$	6.71×10^7
256	$(16 \times 16 \times 1)$	$64 \times 64 \times 1024$	64	$(8 \times 8 \times 1)$	1.34×10^8
			128	$(8 \times 16 \times 1)$	2.68×10^8
512	$(16 \times 32 \times 1)$	$64 \times 32 \times 1024$	256	$(16 \times 16 \times 1)$	5.37×10^8
			512	$(16 \times 32 \times 1)$	1.07×10^9
1024	$(32 \times 32 \times 1)$	$32 \times 32 \times 1024$	1024	$(32 \times 32 \times 1)$	2.15×10^9

by HMFEM is the most expensive part of the algorithm, as we will see in the experiments below. The last column shows the increase percentage in the total number of local problems to be computed.

Table 3: Shows the total number (globally) of MMBFs to be computed in level $\ell = \mathcal{L}$ for the cases where we have $\bar{H} = H$ and $\bar{H} = H/4$.

Subdomains	Number of MMBFS for $\overline{H} = H$	Number of MMBFS for $\overline{H} = H/4$	% increase
$4 \times 8 \times 1$	136	448	330 %
$8 \times 8 \times 1$	288	960	333 %
$8 \times 16 \times 1$	592	1984	335 %
$16 \times 16 \times 1$	1216	4096	337 %
$16 \times 32 \times 1$	2464	8320	338 %
$32 \times 32 \times 1$	4992	16896	338 %

Finally, in the accuracy experiments we show that the accuracy of the approximated flux does not deteriorates as we increase the number of cores for the strong and weak scaling studies. No downscaling strategy was used so that pressure and normal fluxes may be discontinuous at the fine grid across the skeleton of the decomposition. As we are dealing with very large problems, we restricted our simulations to a maximum of 4 million cells per subdomain due to memory and computational restrictions.

5.2. Homogeneous scalability study

For the experiments in this section, we consider an isotropic homogeneous absolute permeability field given by $K(\mathbf{x}) = 1$.

5.2.1. Strong scaling

Figures 7 and 8 present the scalability curves of time ratio versus number of cores. Under ideal conditions, with a fully paralellizable method, we expect the computational time to be reduced by half if we double the number of processing cores, since the computational power was doubled. The red curve represents the ideal scaling curve,

$$\frac{T_{ref}}{T_n} = \frac{n_c}{n_{c_{ref}}}, \tag{37}$$

where T_n is the total time of computation and n_c the number of cores used; while T_{ref} is the reference processing time spent to compute the solution using $n_{c_{ref}}$ cores. The blue curves represent our data.

In Figures 7a and 7b we present the scaling curves for the three-dimensional problem with $512 \times 512 \times 512$ (approximately 134 million) cells and $1024 \times 1024 \times 1024$ (approximately 1 billion) cells, respectively, with computational times reported in Table 4 for the $\bar{H} = H$ case. The same experiments are reported in Figures 8a and 8b as well as in Table 5, for the $\bar{H} = H/4$ case.
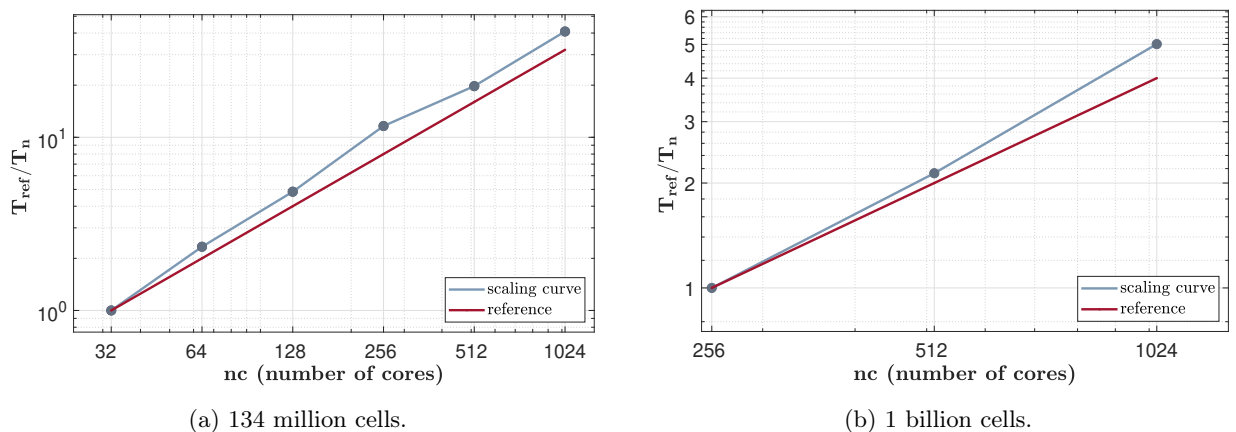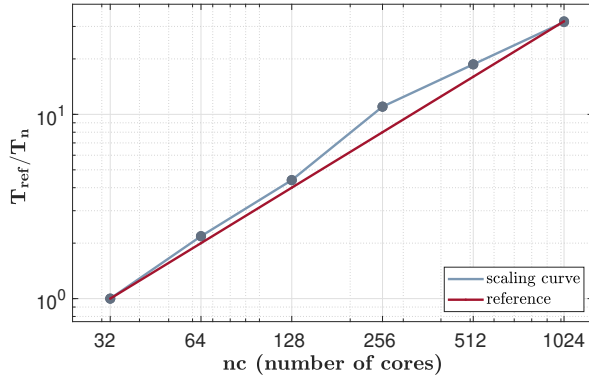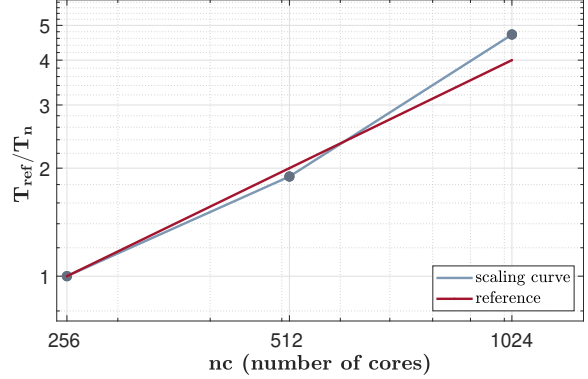

(a) 134 million cells. (b) 1 billion cells.

Figure 7: Strong scaling curves with homogeneous permeability and $\bar{H} = H$ (see Table 4).

17

(a) 134 million cells.

(b) 1 billion cells.

Figure 8: Strong scaling curves with homogeneous permeability and $\bar{H} = H/4$ (see Table 5).

Table 4: Strong scaling times for homogeneous problem with 134 million cells (top table, see Figure 7a) and with 1 billion cells (bottom table, see Figure 7b). For these problems we considered $\bar{H} = H$.

Strong Scaling (homogeneous permeability - $\bar{H} = H$)

134 million cells

Cores	MMBFs Time (s)	INTRF Time (s)	MPI Time (s)	Total Time (s)	% decrease (Total)
32	94.66	0.0071	0.0001	128.84	
64	41.43	0.0072	0.0002	54.88	57.41
128	20.81	0.0048	0.0003	26.15	52.35
256	8.31	0.0063	0.0005	10.75	58.87
512	4.73	0.0082	0.0007	5.98	44.40
1024	1.88	0.0123	0.0024	2.73	54.30

1 billion cells

Cores	MMBFs Time (s)	INTRF Time (s)	MPI Time (s)	Total Time (s)	% decrease (Total)
256	87.107	0.1009	0.0062	116.22	
512	46.195	0.0108	0.0007	54.094	53.46
1024	17.278	0.0151	0.0024	22.858	57.74

We can see from these figures that our simulations are above the optimal (red) curve up to 1024 cores, showing outstanding parallel performance. This behavior can be observed in Tables 4 and 5, which show the times for the total run and for the MMBFs computation on level $\ell = \mathcal{L}$. From these tables, one can see that the most expensive part of the overall computation of the solution is in the construction of the MMBF's, as compared to the total time. The remaining time includes the solution of the interface problems in all levels

Table 5: Strong scaling times for homogeneous problem with 134 million cells (top table, see Figure 8a) and with 1 billion cells (bottom table, see Figure 8b). For these problems we considered $\bar{H} = H/4$.

Strong Scaling (homogeneous permeability - $\bar{H} = H/4$)

134 million cells

Cores	MMBFs Time (s)	INTRF Time (s)	MPI Time (s)	Total Time (s)	% decrease (Total)
32	303.72	0.0226	0.0013	396.36	
64	140.92	0.0240	0.0024	181.40	54.23
128	72.60	0.0553	0.0037	89.74	50.53
256	29.26	0.1596	0.0124	35.66	60.27
512	16.46	0.9026	0.0356	20.66	42.06
1024	6.71	3.9744	0.1262	12.12	41.34

1 billion cells

Cores	MMBFs Time (s)	INTRF Time (s)	MPI Time (s)	Total Time (s)	% decrease (Total)
256	297.61	0.6224	0.0410	362.87	
512	166.59	0.8838	0.0337	191.05	47.35
1024	61.10	3.9706	0.1239	76.67	59.87

of the recursive algorithm as well as the time spent with exchange of information between subdomains. The latter is around three orders of magnitude smaller as compared to the processing times.

5.2.2. Weak scaling

As mentioned before, in an ideal problem (100% parallelizable) we expect a constant overall processing time while increasing problem size, since the degrees of freedom for each local problem are fixed. Scalability curves are reported in Figures 9 and 10, where we can see overall processing time versus number of cores. The reference curve (red curve) is an average of the total times obtained by our simulations, reported by the blue curves.

In Figures 9a and 9b we have the scaling curves with a fixed number of subdomain cells of $64 \times 64 \times 64$ (approximately 262 thousand cells) and $128 \times 128 \times 128$ (approximately 2 million cells) respectively, computed with $\bar{H} = H$. Figures 10a and 10b report the same weak scaling experiments, but now with $\bar{H} = H/4$. The figures show that the computational time of our simulations remains practically constant, which again shows an outstanding parallel performance, at least up to 1024 processing cores.

In Tables 6 and 7 we have the total time and the individual times of the computation of MMBFs, the time spent on the interface problem and the message exchange time between cores. We can see that the total time is essentially constant. The time for the exchange of information and the time for the interface problem
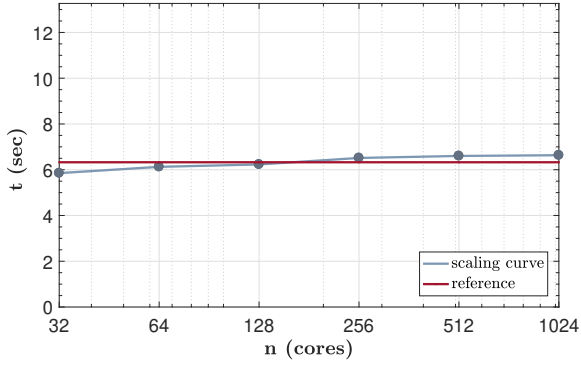
(a) 262 thousand cells per subdomain.
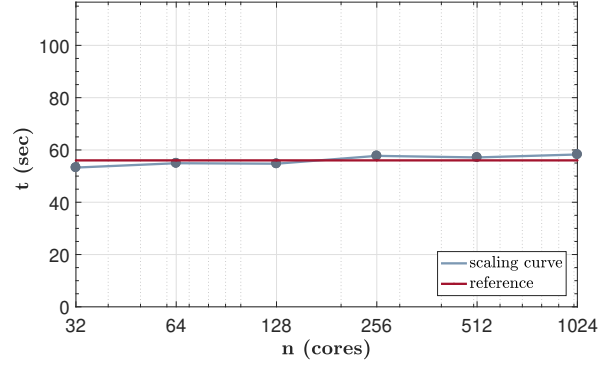
(b) 2 million cells per subdomain.

Figure 9: Weak scaling curves with homogeneous permeability and $\bar{H} = H$ (see Table 6).
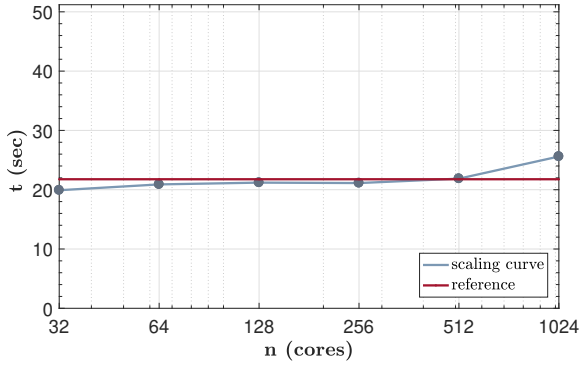
(a) 262 thousand cells per subdomain.
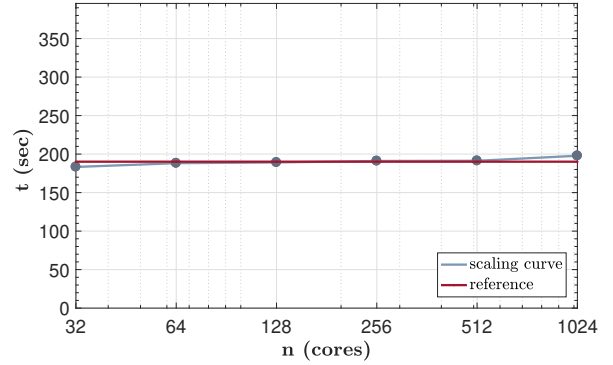
(b) 2 million cells per subdomain.

Figure 10: Weak scaling curves with homogeneous permeability and $\bar{H} = H/4$ (see Table 7).

are very small, resulting in excellent parallel performance. There is a slight increase in computational time for the largest cases (1024 processing cores), which is related to the computation of the MMBFs by iterative methods. An important feature of this implementation is the small computational time of the interface problem compared to the local problems, and this is clearly seen in Table 7. The size and the quantity of interface linear systems to be solved at each level depends directly on the number of $\bar{H}$ partitions at the interface. The problem with $\bar{H} = H$, which translates to one $\bar{H}$ partition at each subdomain interface, results in an interface linear system of size 2×2 in level $\ell = \mathcal{L}$, doubling its size for each previous level. These systems are small enough to be solved efficiently by a direct solver based on LU decomposition. Also, each set of interface linear systems are solved simultaneously within each core, which accelerates the mixed multiscale method. Now, the total number of interface problems to be solved on all levels depends on both the number of $\bar{H}$ partitions and the number of cores. This means that the more levels we have, more time we are going to spend in the computation of the interface problems. This behavior is reported in Tables 6

20

and 7, for a fixed $\bar{H}$. Despite this increase, the time spent on interface calculations is still negligible compare to the total time in the examples considered here.

Table 6: Weak scaling times for homogenous problem with 262 thousand cells (top table, see Figure 9a) and 2 million cells (bottom table, see Figure 9b) per subdomain. For these problems we considered $\bar{H} = H$.

Weak Scaling (homogeneous permeability - $\bar{H} = H$)

262 thousand cells per subd.

Cores	MMBFs Time (s)	INTRF Time (s)	MPI Time (s)	Total Time (s)	% Avg. dev.
32	4.21	0.0012	0.0001	5.85	6.60
64	4.47	0.0014	0.0002	6.13	2.22
128	4.67	0.0058	0.0003	6.23	0.54
256	4.83	0.0022	0.0004	6.51	3.98
512	5.17	0.0112	0.0007	6.60	5.38
1024	5.79	0.0922	0.0760	6.99	9.48

2 million cells per subd.

Cores	MMBFs Time (s)	INTRF Time (s)	MPI Time (s)	Total Time (s)	% Avg. dev.
32	38.87	0.0034	0.0001	53.26	4.14
64	42.24	0.0036	0.0002	54.93	1.14
128	43.42	0.0039	0.0004	54.74	1.48
256	44.21	0.0047	0.0005	57.74	3.92
512	47.42	0.0070	0.0008	57.14	2.84
1024	53.32	0.0893	0.0757	58.69	4.65

Table 7: Weak scaling times for homogeneous problem with 262 thousand cells (top table, see Figure 10a) and 2 million cells (bottom table, see Figure 10b) per subdomain. For these problems we considered $\bar{H} = H/4$.

Weak Scaling (homogeneous permeability - $\bar{H} = H/4$)

262 thousand cells per subd.

Cores	MMBFs Time (s)	INTRF Time (s)	MPI Time (s)	Total Time (s)	% Avg. dev.
32	15.08	0.0064	0.0006	19.91	5.16
64	16.05	0.0120	0.0023	20.89	0.49
128	16.15	0.0454	0.0039	21.19	0.93
256	16.35	0.1582	0.0110	21.12	0.59
512	17.79	0.8692	0.0368	21.87	4.13
1024	20.69	4.2895	0.3349	26.05	19.29

2 million cells per subd.

Cores	MMBFs Time (s)	INTRF Time (s)	MPI Time (s)	Total Time (s)	% Avg. dev.
32	139.88	0.0132	0.0010	183.30	2.81
64	149.86	0.0194	0.0024	188.18	0.22
128	151.23	0.0525	0.0043	189.17	0.30
256	153.83	0.1618	0.0119	191.05	1.30
512	165.33	0.8364	0.0355	191.28	1.42
1024	188.91	4.1823	0.4077	198.29	4.25

5.3. Heterogeneous scalability study

For the heterogeneous permeability field, we use a log-normal model for multiscale rock heterogeneity proposed by Glimm and Sharp [36] where the absolute permeability is given by

$$K(\mathbf{x}) = K_0 \exp(\omega_K \xi(\mathbf{x})), \tag{38}$$

where $\xi(\mathbf{x})$ is an independent Gaussian field with $K_0 = 1.6487$ and $\omega_K = 3.7$ in order to generate a permeability field with contrast $K_{max}/K_{min} = 10^8$ on a mesh of $60 \times 60 \times 60$ cells. For simulations in finer grid resolutions, the same permeability field is used by projecting it onto the finer grids. In Figure 11 we illustrate the three-dimensional heterogeneous absolute permeability used for the scaling experiments, and a two-dimensional slice in the middle of the z-direction that was used for the accuracy experiments.
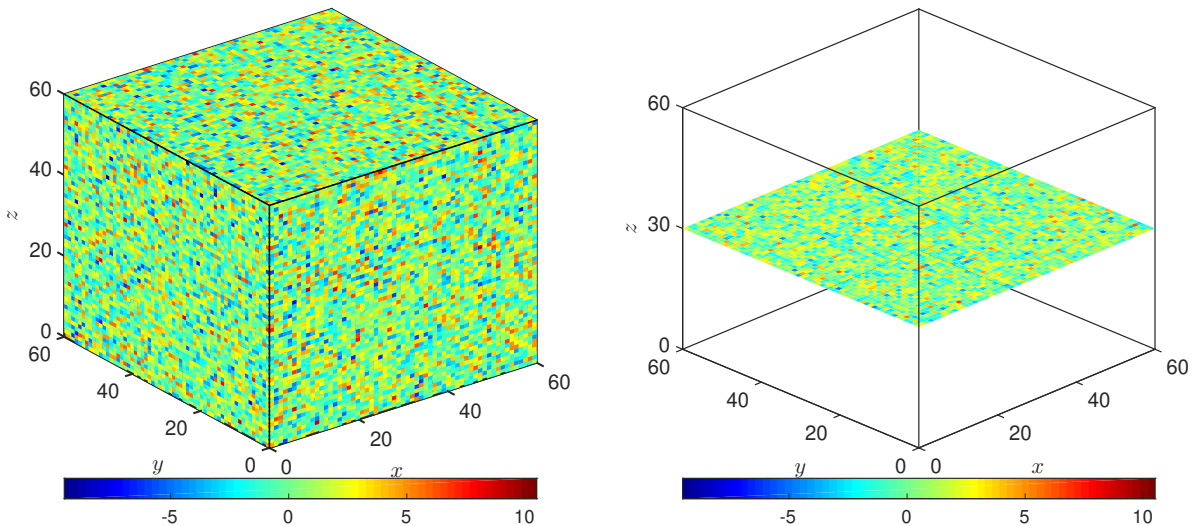
Figure 11: The left picture shows the three-dimensional heterogeneous permeability with a contrast of 10^8 given by (38). The right picture shows a two-dimensional slice on the middle of the z-direction of the permeability on the left.

5.3.1. Strong scaling

For the heterogeneous experiments we considered the same conditions as homogeneous strong scaling experiments. In Figures 12a and 12b, and Table 8 we present the scaling curves and computational times for the $\bar{H} = H$ problem with total 134 million and 1 billion cells, respectively. In Figures 13a and 13b, and Table 9 we show the experiments considering $\bar{H} = H/4$. We can see that our simulations again exhibit excellent performance. The times for the interface problem remain negligible.
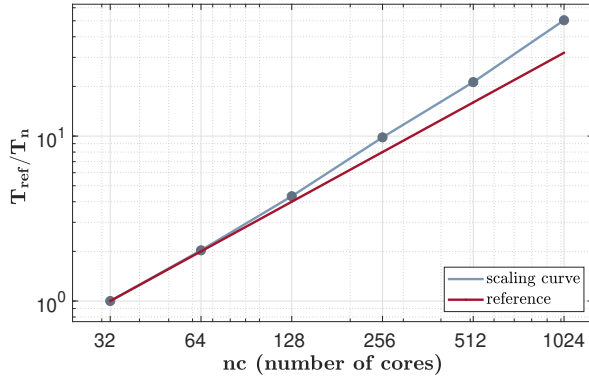
(a) 134 million cells.
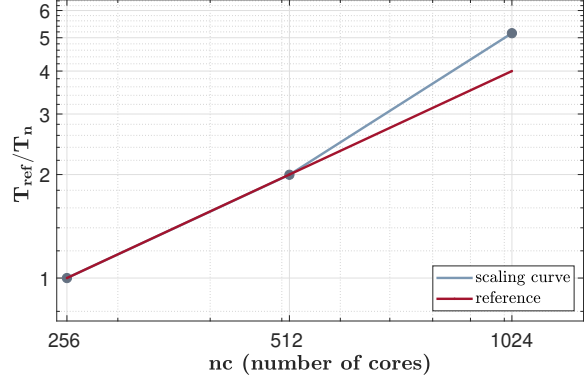
(b) 1 billion cells.

Figure 12: Strong scaling curves with heterogeneous log-normal permeability and $\bar{H} = H/4$ (see Table 8).

(a) 134 million cells.
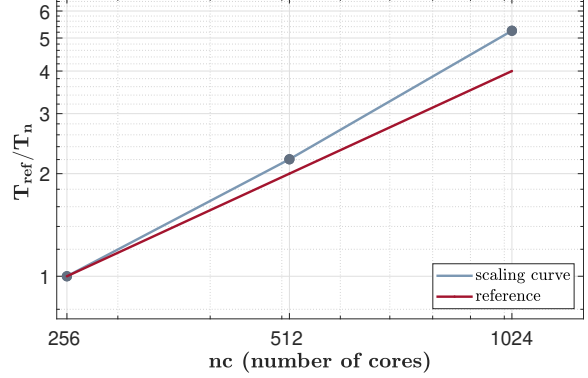
(b) 1 billion cells.

Figure 13: Strong scaling curves with heterogeneous log-normal permeability and $\bar{H} = H/4$ (see Table 9).

5.3.2. Weak scaling

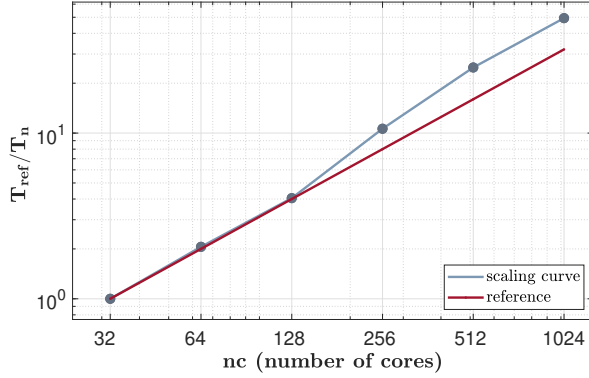For these experiments we considered the same conditions as the previous experiments of weak scaling but with the same permeability of the heterogeneous strong scaling study. The heterogeneous permeability field is repeated on each subdomain to reproduce the same experiment performed for the homogeneous weak scaling. We also use the same nondimensionalized boundary conditions. Notice that the for each set of processors we solve a different heterogeneous problem. The idea is to keep the same computational effort on each subdomain and assess the method behavior especially for the interface problems.

In Figures 14a and 14b we have the scaling curves for the heterogeneous problem with $\bar{H} = H$ and a fixed number of subdomain cells of 262 thousand and 2 million cells respectively. In Figures 15a and 15b we show the same weak scaling experiments with $\bar{H} = H/4$. Tables 10 and 11 shows the computational times and we can see that the runtime is fairly close. The variation in time that we see is related to the fact

24

Table 8: Strong scaling for heterogeneous problem with 134 million cells (top table, see Figure 12a) and with 1 billion cells (bottom table, see Figure 12b). For these problems we considered $\bar{H} = H$.

Strong Scaling (heterogeneous $\bar{H} = H$)

134 million cells

Cores	MMBFs Time (s)	INTRF Time (s)	MPI Time (s)	Total Time (s)	% decrease (Total)
32	303.99	0.0225	0.0077	398.33	
64	143.84	0.0055	0.0002	195.96	50.80
128	64.88	0.0659	0.0004	91.81	53.15
256	24.48	0.0037	0.0005	40.21	56.21
512	11.10	0.0060	0.0007	18.21	54.71
1024	3.85	0.0123	0.0023	7.48	58.91

1 billion cells

Cores	MMBFs Time (s)	INTRF Time (s)	MPI Time (s)	Total Time (s)	% decrease (Total)
256	207.53	0.0110	0.0007	328.40	
512	99.21	0.0121	0.0008	164.05	50.05
1024	33.18	0.0156	0.0024	63.37	61.37

Table 9: Strong scaling times for heterogeneous problem with 134 million cells (top table, see Figure 13a) and with 1 billion cells (bottom table, see Figure 13b). For these problems we considered $\bar{H} = H/4$.

Strong Scaling (heterogeneous $\bar{H} = H/4$)

134 million cells

Cores	MMBFs Time (s)	INTRF Time (s)	MPI Time (s)	Total Time (s)	% decrease (Total)
32	1102.10	0.1650	0.0540	1389.00	
64	507.26	0.0255	0.0024	674.43	51.44
128	233.85	0.0558	0.0036	342.57	49.21
256	86.87	0.1587	0.0123	130.41	61.93
512	39.98	0.8985	0.0350	55.24	57.64
1024	15.80	4.2353	0.1949	27.51	50.21

1 billion cells

Cores	MMBFs Time (s)	INTRF Time (s)	MPI Time (s)	Total Time (s)	% decrease (Total)
256	712.82	0.1820	0.0130	1044.30	
512	351.85	0.8917	0.0337	473.37	54.67
1024	131.19	4.0390	0.2042	198.25	58.12

that we solve different problems at each point since we repeat the permeability in each subdomain. Still, the influence of the MMBFs computation dominates the total time. The computation time of the interface problems continue to have little influence on the total time and follows the same increase pattern of the homogeneous problem as we consider the same number of $\bar{H}$ partitions and levels. This shows that the interface time is insensible to changes in the permeability.
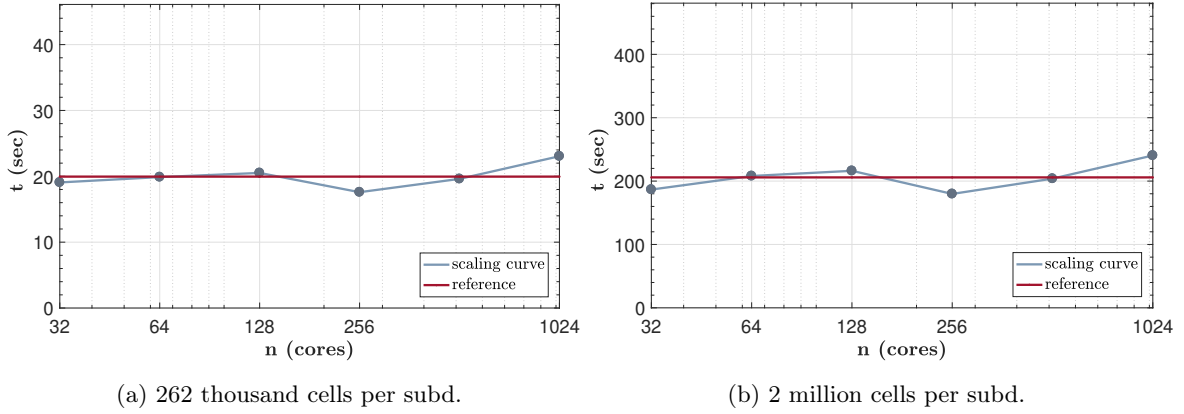

(a) 262 thousand cells per subd.

(b) 2 million cells per subd.

Figure 14: Weak scaling curves with heterogeneous log-normal permeability and $\bar{H} = H$ (see Table 10).

(a) 262 thousand cells per subd.
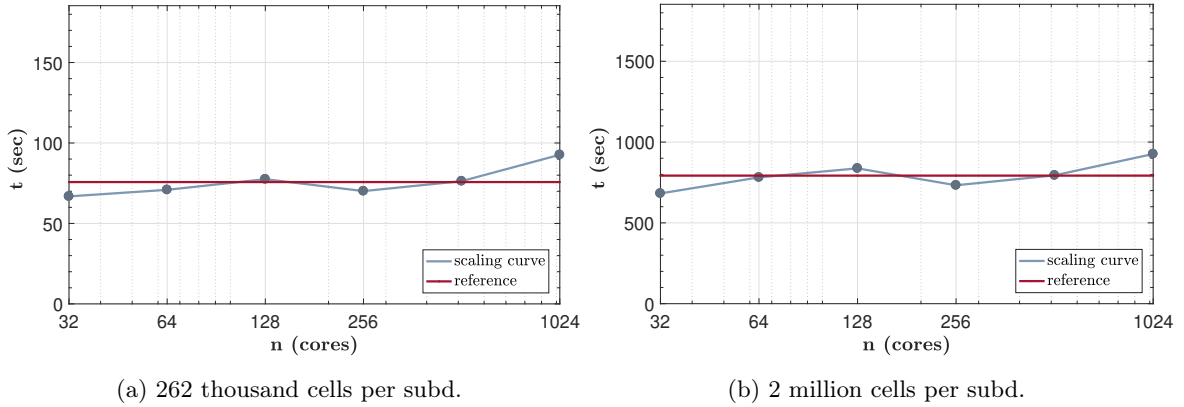
(b) 2 million cells per subd.

Figure 15: Weak scaling curves with heterogeneous log-normal permeability and $\bar{H} = H/4$ (see Table 11).

26

Table 10: Weak scaling times for heterogeneous problem with 262 thousand cells (top table, see Figure 14a) and 2 million cells (bottom table, see Figure 14b) per subdomain. For these problems we considered $\bar{H} = H$.

Weak Scaling (heterogeneous $\bar{H} = H$)

262 thousand cells per subd.

Cores	MMBFs Time (s)	INTRF Time (s)	MPI Time (s)	Total Time (s)	% Avg. dev.
32	18.22	0.0012	0.0001	19.42	4.78
64	18.84	0.0017	0.0002	20.36	0.17
128	19.47	0.0021	0.0004	21.00	2.97
256	16.67	0.0028	0.0006	17.98	11.84
512	18.42	0.0158	0.0051	20.16	1.15
1024	21.93	0.0813	0.0334	23.45	14.98

2 million cells per subd.

Cores	MMBFs Time (s)	INTRF Time (s)	MPI Time (s)	Total Time (s)	% Avg. dev.
32	181.89	0.0037	0.0001	186.98	9.35
64	203.14	0.0043	0.0002	208.53	1.10
128	211.49	0.0046	0.0006	216.69	5.06
256	174.90	0.0123	0.0044	180.12	12.67
512	198.65	0.0138	0.0015	204.43	0.89
1024	235.34	0.0232	0.0085	240.82	16.75

Table 11: Weak scaling times for heterogeneous problem with 262 thousand cells (top table, see Figure 15a) and 2 million cells (bottom table, see Figure 15b) per subdomain. For these problems we considered $\bar{H} = H/4$.

Weak Scaling (heterogeneous $\bar{H} = H/4$)

262 thousand cells per subd.

Cores	MMBFs Time (s)	INTRF Time (s)	MPI time (s)	Total Time (s)	% Avg. dev.
32	65.95	0.0056	0.0007	67.18	11.66
64	69.83	0.0132	0.0026	71.38	6.14
128	76.43	0.0491	0.0054	78.01	2.58
256	68.94	0.2126	0.0545	70.47	7.33
512	73.67	1.4458	0.0692	76.89	1.11
1024	87.35	4.4946	0.5147	93.20	22.55

2 million cells per subd.

Cores	MMBFs Time (s)	INTRF Time (s)	MPI Time (s)	Total Time (s)	% Avg. dev.
32	677.54	0.0131	0.0013	682.59	13.87
64	776.62	0.0222	0.0033	782.04	1.32
128	832.58	0.0552	0.0052	837.85	5.72
256	727.69	0.2032	0.0454	733.13	7.49
512	787.45	1.4758	0.0782	794.79	0.29
1024	917.05	4.2828	0.5280	926.82	16.95

5.4. Velocity accuracy in scaling studies

In this section we present a study on the velocity field error to assess the behavior of the solution as we increase the number of cores. In all studies we compute the accuracy of the flux compared to a reference solution. The problems presented are two-dimensional slices of the strong and weak scalings three-dimensional experiments reported above. We compute $||\mathbf{u} - \mathbf{u}_h||_{L^2(\Omega)}/||\mathbf{u}||_{L^2(\Omega)}$, the $L^2(\Omega)$ relative velocity error norm, where $\mathbf{u}$ is the reference solution obtained by a hybrid mixed finite element discretization [31, 33] with the same AMG solver [35] used to solve the resulting linear system for the pressure.

In Tables 12 and 13 we present the relative velocity error norms of the two-dimensional slice of the strong scaling problems with 134 million cells for the homogeneous permeability and heterogeneous permeability (see Figure 11), respectively. The errors shown are obtained both for $\bar{H} = H$ and $\bar{H} = H/4$. The tables indicate that as the core number increases (and consequently the number of levels increases) the approximated solution does not deteriorate.

Table 12: A two-dimensional flux accuracy study for homogeneous problem with 262 thousand cells. The problem represents a two-dimensional slice of the homogeneous strong scaling problem (4) and (5) with 134 million cells.

		262 thousand cells (homogeneous permeability)	
	Subd. cells	$\bar{H} = H$	$\bar{H} = H/4$
Cores	$(n_x \times n_y \times n_z)$	$||\mathbf{u} - \mathbf{u}_h||_2/||\mathbf{u}||_2$	$||\mathbf{u} - \mathbf{u}_h||_2/||\mathbf{u}||_2$
32	$128 \times 64 \times 1$	5.21e-05	6.02e-06
64	$64 \times 64 \times 1$	1.01e-05	1.11e-06
128	$64 \times 32 \times 1$	2.69e-05	3.11e-06
256	$32 \times 32 \times 1$	5.16e-06	5.95e-07
512	$32 \times 16 \times 1$	1.35e-05	1.58e-06
1024	$16 \times 16 \times 1$	2.56e-06	3.10e-07

In Tables 14 and 15 we show the relative flux errors for a slice of the weak scaling problem with 262 thousand cells per subdomain. In Table 14 we present the errors for the homogeneous permeability problem and in Table 15 we present the errors for the heterogeneous permeability, both for the two-dimensional slice with $64 \times 64 \times 1$ cells per subdomain. For the heterogeneous problems the slice shown in Figure 11 is repeated in each subdomain, using the same strategy as the weak scaling experiments above. The errors are again obtained both for $\bar{H} = H$ and $\bar{H} = H/4$. The tables indicate that as the core number increases there are no loss of accuracy in the approximated solution.

6. Discussion

To the best of our knowledge, there are very few weak and strong scaling results for parallel implementations of multiscale methods in the literature for three dimensional heterogeneous Darcy's flow and

Table 13: A two-dimensional flux accuracy study for heterogeneous problem with 262 thousand cells. The problem represents a two-dimensional slice of the heterogeneous strong scaling problem (8) and (9) with 134 million cells.

262 thousand cells (heterogeneous permeability)

Cores	Subd. cells $(n_x \times n_y \times n_z)$	$\bar{H} = H$ $\|\mathbf{u} - \mathbf{u}_h\|_2/\|\mathbf{u}\|_2$	$\bar{H} = H/4$ $\|\mathbf{u} - \mathbf{u}_h\|_2/\|\mathbf{u}\|_2$
32	$128 \times 64 \times 1$	5.60e-01	4.02e-01
64	$64 \times 64 \times 1$	6.70e-01	4.26e-01
128	$64 \times 32 \times 1$	6.55e-01	3.95e-01
256	$32 \times 32 \times 1$	7.10e-01	3.87e-01
512	$32 \times 16 \times 1$	7.04e-01	3.27e-01
1024	$16 \times 16 \times 1$	7.20e-01	2.87e-01

Table 14: A two-dimensional flux accuracy study 1.2 for homogeneous problem with 4096 cells. The problem represents a two-dimensional slice of the homogeneous weak scaling problem (6) and (7) with 262 thousand cells per subdomain.

4096 cells per subd. (homogeneous permeability)

Cores	Subd. cells $(n_x \times n_y \times n_z)$	$\bar{H} = H$ $\|\mathbf{u} - \mathbf{u}_h\|_2/\|\mathbf{u}\|_2$	$\bar{H} = H/4$ $\|\mathbf{u} - \mathbf{u}_h\|_2/\|\mathbf{u}\|_2$
32	$64 \times 64 \times 1$	9.87e-06	1.11e-06
64	$64 \times 64 \times 1$	1.01e-05	1.11e-06
128	$64 \times 64 \times 1$	1.04e-05	1.16e-06
256	$64 \times 64 \times 1$	1.05e-05	1.17e-06
512	$64 \times 64 \times 1$	1.06e-05	1.20e-06
1024	$64 \times 64 \times 1$	1.06e-05	1.23e-06

two-phase flow problems (see, [12, 13, 14, 15, 16]). In most of these papers the authors consider a small number of processing cores (up to 20), except in [16] that went up to 256 cores in 16 nodes, and numerical simulations with at most hundreds of millions of cells which are comparable to our smallest simulations. In addition, in these papers the most extensive scalability study for multiscale methods is made for an algebraic extension of multiscale methods [12, 13, 14] that uses the multiscale method as a preconditioner to damp low/high frequency modes of the resulting discretized linear system related to the underlying elliptic PDE. It is noteworthy that in this work we consider very large problems that can have billions of cells, motivated by the numerical simulation of subsurface flows, making use of a MPI base code for up to 1024 processing cores on 22 nodes. The numerical experiments reported in the above mentioned papers are restricted to 128 million cells for both GPU [14] and CPU shared-memory architecture up to 20 processing cores on a single node [12, 13]. In the study of [16] that make use of 256 processing cores, the three-dimensional simulations

Table 15: A two-dimensional flux accuracy study for heterogeneous problem with 4096 cells. The problem represents a two-dimensional slice of the heterogeneous weak scaling problem (10) and (11) with 262 thousand cells per subdomain.

		4096 cells per subd. (heterogeneous permeability)	
Cores	Subd. cells $(n_x \times n_y \times n_z)$	$\bar{H} = H$ $\|\mathbf{u} - \mathbf{u}_h\|_2/\|\mathbf{u}\|_2$	$\bar{H} = H/4$ $\|\mathbf{u} - \mathbf{u}_h\|_2/\|\mathbf{u}\|_2$
32	$64 \times 64 \times 1$	7.91e-01	6.72e-01
64	$64 \times 64 \times 1$	9.12e-01	8.77e-01
128	$64 \times 64 \times 1$	8.54e-01	3.75e-01
256	$64 \times 64 \times 1$	7.98e-01	2.67e-01
512	$64 \times 64 \times 1$	6.20e-01	3.79e-01
1024	$64 \times 64 \times 1$	6.24e-01	4.23e-01

considered problems with about 16 million discretized cells. Our results though, considered a larger set of nodes with an excellent strong and weak scalability up to 1024 processing cores reaching up to 2 billion cells in the weak scaling study and 1 billion in the strong scaling study.

7. Concluding Remarks

In this paper we developed a recursive formulation for the Multiscale Robin Coupled Method that can be extended to the family of mixed multiscale methods that the MRCM encompasses. The original global interface problem was replaced by a set of small interface linear systems associated with adjacent subdomains, in a hierarchy built as unions of nearest neighbor subdomains. A novel parallel algorithm is introduced and implemented for very large (up to 2 billions cells) problems, motivated by the numerical simulation of subsurface flows. The recursive formulation was built to solve the global coarse algebraic problem more efficiently maintaining the features of the underlying multiscale method. Through several numerical studies for both homogeneous and highly heterogeneous permeability fields we showed that the new algorithm is very fast and exhibits excellent scaling, with superlinear profile. As expected, the highly heterogeneous problems present an increase of computational time compared to the equivalent homogeneous problems. We observed small times for the numerical solution of the interface problem, with the computation of the local boundary problems prevailing over the total computational time in all cases. Also, small changes on the intermediate coarse scale did not affect the scalability of the formulation. The simulations were performed up to 1024 processing cores without deterioration of the velocity field accuracy presenting realistic potential of application in very large and highly heterogeneous reservoirs.

Acknowledgments

References

[1] T. Y. Hou, X. H. Wu, A multiscale finite element method for elliptic problems in composite materials and porous media, Journal of Computational Physics 134 (1) (1997) 169–189.

[2] Y. Efendiev, T. Y. Hou, Multiscale finite element methods: theory and applications, Vol. 4, Springer Science & Business Media, 2009.

[3] Y. Efendiev, J. Galvis, T. Y. Hou, Generalized multiscale finite element methods (GMsFEM), Journal of Computational Physics 251 (2013) 116–135.

[4] P. Jenny, S. H. Lee, H. A. Tchelepi, Multi-scale finite-volume method for elliptic problems in subsurface flow simulation, Journal of Computational Physics 187 (1) (2003) 47–67.

[5] P. Jenny, S. H. Lee, H. A. Tchelepi, Adaptive multiscale finite-volume method for multiphase flow and transport in porous media, Multiscale Modeling & Simulation 3 (1) (2005) 50–64.

[6] S. H. Lee, C. Wolfsteiner, H. A. Tchelepi, Multiscale finite-volume formulation for multiphase flow in porous media: black oil formulation of compressible, three-phase flow with gravity, Computational Geosciences 12 (3) (2008) 351–366.

[7] I. Lunati, P. Jenny, Multiscale finite-volume method for compressible multiphase flow in porous media, Journal of Computational Physics 216 (2) (2006) 616 – 636.

[8] P. Jenny, I. Lunati, Modeling complex wells with the multi-scale finite-volume method, Journal of Computational Physics 228 (3) (2009) 687 – 702.

[9] I. Sokolova, G. B. Muhammad, H. Hajibeygi, Multiscale finite volume method for finite-volume-based simulation of poroelasticity, Journal of Computational Physics 379 (2019) 309 – 324.

[10] H. Hajibeygi, G. Bonfigli, M. A. Hesse, P. Jenny, Iterative multiscale finite-volume method, Journal of Computational Physics 227 (19) (2008) 8604–8621.

[11] H. Hajibeygi, P. Jenny, Adaptive iterative multiscale finite volume method, Journal of Computational Physics 230 (3) (2011) 628–643.

[12] A. M. Manea, J. Sewall, H. A. Tchelepi, Parallel multiscale linear solver for highly detailed reservoir models, SPE Journal 21 (06) (2016) 2–062.

[13] A. M. Manea, H. Hajibeygi, P. Vassilevski, H. A. Tchelepi, Parallel enriched algebraic multiscale solver, in: SPE Reservoir Simulation Conference, Society of Petroleum Engineers, 2017.

[14] A. M. Manea, T. Almani, A massively parallel algebraic multiscale solver for reservoir simulation on the GPU architecture, in: SPE Reservoir Simulation Conference, Society of Petroleum Engineers, 2019.

[15] N. Zhang, B. Yan, Q. Sun, Y. Wang, Improving multiscale mixed finite element method for flow simulation in highly heterogeneous reservoir using adaptivity, Journal of Petroleum Science and Engineering 154 (2017) 382–388.

[16] M. A. Puscas, G. Enchéry, S. Desroziers, Application of the mixed multiscale finite element method to parallel simulations of two-phase flows in porous media, Oil & Gas Science and Technology–Revue d'IFP Energies nouvelles 73 (2018) 38.

[17] T. Arbogast, G. Pencheva, M. F. Wheeler, I. Yotov, A multiscale mortar mixed finite element method, Multiscale Modeling & Simulation 6 (1) (2007) 319–346.

[18] B. Ganis, I. Yotov, Implementation of a mortar mixed finite element method using a multiscale flux basis, Computer Methods in Applied Mechanics and Engineering 198 (49-52) (2009) 3989–3998.

[19] M. F. Wheeler, G. Xue, I. Yotov, A multiscale mortar multipoint flux mixed finite element method, ESAIM: Mathematical Modelling and Numerical Analysis 46 (4) (2012) 759–796.

[20] E. Ahmed, A. Fumagalli, A. Budisa, A multiscale flux basis for mortar mixed discretizations of reduced Darcy-Forchheimer fracture models, Computer Methods in Applied Mechanics and Engineering 354 (2019) 16 – 36.

[21] R. Araya, C. Harder, D. Paredes, F. Valentin, Multiscale Hybrid-Mixed Method, SIAM Journal on Numerical Analysis 51 (6) (2013) 3505–3531.

[22] C. Harder, D. Paredes, F. Valentin, A family of multiscale hybrid-mixed finite element methods for the Darcy equation with rough coefficients, Journal of Computational Physics 245 (2013) 107 – 130.

[23] R. Araya, C. Harder, H. A. Poza, F. Valentin, Multiscale Hybrid-Mixed Method for the Stokes and Brinkman equations – the method, Computer Methods in Applied Mechanics and Engineering 324 (2017) 29 – 53.

[24] A. Francisco, V. Ginting, F. Pereira, R. J., Design and implementation of a multiscale mixed method based on a nonoverlapping domain decomposition procedure, Mathematics and Computers in Simulation 99 (2014) 125–138.

[25] H. Akbari, A. Engsig-Karup, V. Ginting, F. Pereira, A multiscale direct solver for the approximation of flows in high contrast porous media, Journal of Computational and Applied Mathematics 359 (2009) 5129 – 5147.

[26] R. T. Guiraldello, R. F. Ausas, F. S. Sousa, F. Pereira, G. C. Buscaglia, The Multiscale Robin Coupled Method for flows in porous media, Journal of Computational Physics 355 (2018) 1–21.

[27] R. T. Guiraldello, R. F. Ausas, F. S. Sousa, F. Pereira, G. C. Buscaglia, Interface spaces for the Multiscale Robin Coupled Method in reservoir simulation, Mathematics and Computers in Simulation 164 (2019) 103 – 119.

[28] J. Douglas, P. J. P. Leme, J. E. Roberts, J. Wang, A parallel iterative procedure applicable to the approximate solution of second order partial differential equations by mixed finite element methods, Numerische Mathematik 65 (1) (1993) 95–108.

[29] P. Ferraz, A novel recursive formulation of multiscale mixed methods and relaxation modeling of flow in porous media, Ph.D. thesis, IMECC/University of Campinas (July 2019).

[30] F. F. Rocha, F. S. Sousa, R. F. Ausas, G. C. Buscaglia, F. Pereira, Multiscale mixed methods for two-phase flows in high-contrast porous media, Journal of Computational Physics 409 (2020) 109316.

[31] J. M. Thomas, P. A. Raviart, A mixed finite element method for second order elliptic problems, In: Lecture Notes in Mathematics (1977) 292–315.

[32] E. Abreu, Numerical modelling of three-phase immiscible flow in heterogeneous porous media with gravitational effects, Mathematics and Computers in Simulation 97 (2014) 234–259.

[33] J. E. Roberts, Mixed and Hybrid methods, Handbook of Numerical Analysis, Vol II, Finite Element Methods (Part 1) (1991) 523–633.

[34] R. T. Guiraldello, R. F. Ausas, F. S. Sousa, F. Pereira, G. C. Buscaglia, Velocity postprocessing schemes for multiscale mixed methods applied to contaminant transport in subsurface flows, Computational Geosciences (2020) 1–21.

[35] M. Liebmann, Parallel toolbox: Algebraic multigrid preconditioner, last access in august 2019.
URL http://paralleltoolbox.sourceforge.net/

[36] J. Glimm, D. H. Sharp, A random field model for anomalous diffusion in heterogeneous porous media, Journal of Statistical Physics 62 (1-2) (1991) 415–424.